Precambrian Research 430 (2025) 107916

Contents lists available at ScienceDirect

Precambrian Research

journal homepage: www.elsevier.com/locate/precamres

Sedimentology, petrography, and carbon isotopes of the ~2.2 Ga Randville Dolomite, Upper Peninsula of Michigan

Garrett D. Brown [a,b,1], Maya L. Giannecchini [c], Cory M. Redman [d], Ian Z. Winkelstern [c], Dylan T. Wilmeth [c,*]

[a] Department of Plant Biology, Michigan State University, East Lansing, MI 48824, United States
[b] Department of Biology, Grand Valley State University, Grand Rapids, MI 49401, United States
[c] Department of Geology, Grand Valley State University, Grand Rapids, MI 49401, United States
[d] Grand Rapids Public Museum, Grand Rapids, MI 49504, United States

A B S T R A C T

The Lomagundi–Jatuli Event (LJE) was Earth's longest (2.3–2.0 Ga) and largest (+5 to +30 ‰) positive $\delta^{13}C$ excursion. The LJE's exact causes remain uncertain, with various hypotheses involving increased organic carbon burial or restricted depositional facies. While many LJE carbonates have enriched $\delta^{13}C$ signatures, several locations are closer to average values over Earth history (~0‰), providing opportunities to test depositional models. For example, the ~2.2 Ga Randville Dolomite in Michigan's Upper Peninsula is less enriched in $\delta^{13}C$ (0 to +3 ‰) compared to the neighboring Kona Dolomite (+5 to +10 ‰). Randville age constraints are broad but fall within the LJE (2.3–2.1 Ga), approximately coeval with Kona deposits (2.17 Ga). The Randville Dolomite contains extensive planar beds with minor scour-fill structures, slumps, and conglomerates, indicating a relatively calm depositional environment punctuated by storms and slope failures on an outer carbonate platform. Randville deposits contain a variety of microbialites including domal, inclined, nodular, and conical stromatolites, and potentially the oldest recorded dendrolites. The most likely explanation for $\delta^{13}C$ differences between the Randville and Kona Dolomite involves depositional environments. Many enriched Kona deposits represent an evaporitic, marine basin, while Randville facies show little to no evidence for subaerial exposure or evaporation. Facies-dependent patterns between Randville and Kona Dolomites are mirrored in LJE carbonates across the Lake Superior region: formations with evaporites are consistently $\delta^{13}C$-enriched compared with other localities. These datasets support previous research indicating that at least during certain intervals, LJE excursions were not ubiquitous in all marine environments.

1. Introduction

During the Paleoproterozoic (2.5–1.6 Ga), Earth experienced many unique shifts in global geochemistry. One significant change during this interval was the Lomagundi Jatuli Event (LJE), Earth's longest positive carbon isotope excursion (2.3–2.0 Ga) (Schidlowski et al., 1975, Karhu & Holland, 1996; Melezhik et al., 1999; Prave et al., 2022; Hodgskiss et al., 2023). During this time, inorganic $\delta^{13}C$ in many marine carbonate deposits shifted from typical values ~0 ‰ to some of the highest recorded in carbonate deposits (+5 to +30 ‰). The LJE's causes remain debated after 50 years of research, with several potential explanations proposed. The canonical model invokes increased burial and sequestration of ^{13}C-depleted organic material between 2.3–2.0 Ga (Karhu & Holland, 1996; Melezhik et al., 1999; Bekker & Holland, 2012). Assuming relatively constant fluxes and $\delta^{13}C$ values (−6‰) for marine hydrothermal inputs, the $\delta^{13}C$ signature of marine dissolved inorganic carbon (DIC) is dependent on the carbon fixation into organic biomass. Carbon fixation preferentially uptakes ^{12}C; the subsequent burial of organic carbon enriches dissolved inorganic carbon (DIC) in heavier ^{13}C, preserved in carbonate deposits such as limestones and dolostones. For example, modern $\delta^{13}C_{DIC}$ values around 0 ‰ result from ~20 % of total carbon burial as organic matter vs. ~80 % as carbonate minerals (Schidlowski et al., 1975). For most of Earth history, carbonate deposits record similar $\delta^{13}C$ values around 0 ‰. For most of Earth history, carbonate deposits record similar $\delta^{13}C$ values ~0 ‰. According to burial models, elevated $\delta^{13}C$ in LJE carbonates requires increased organic carbon burial, potentially up to 60 % total carbon burial (Schidlowski et al., 1975; Karhu & Holland, 1996). In the Paleoproterozoic, such burial could have been triggered by preceding continental growth and the Great Oxidation Event (GOE, 2.3–2.0 Ga). As atmospheric O_2 increased and terrestrial surfaces grew, surficial weathering potentially enhanced nutrient fluxes into marine environments. More nutrients likely boosted primary productivity, creating more biomass to be buried (Bekker & Holland, 2012). Continental growth also promoted shallow

* Corresponding author.
E-mail address: wilmethd@gvsu.edu (D.T. Wilmeth).
[1] Present address: Department of Plant Biology, Michigan State University, East Lansing, MI 48824, United States.

https://doi.org/10.1016/j.precamres.2025.107916
Received 14 May 2025; Received in revised form 13 August 2025; Accepted 4 September 2025
Available online 16 September 2025

shelf environments with higher sedimentation rates, more easily burying and sequestering isotopically light organic carbon.

While organic burial remains the most widely accepted LJE model, several aspects remain unresolved. The relative timing between continental growth, the GOE, and the LJE is still unclear. The extent of early continental crust remains debated, with some estimates placing enhanced growth well before the LJE (Hawkesworth et al., 2019; Tang et al., 2021). Many deposits bearing GOE and LJE signatures have relatively poor age constraints, obscuring the timing between rising O_2 and $\delta^{13}C$ (Hodgskiss et al., 2023). Furthermore, the enhanced burial of organic matter required to sustain the LJE is not observed in the rock record until the interval's end (Karhu & Holland, 1996; Hodgskiss et al., 2023). These uncertainties have led to alternate, potentially non-exclusive hypotheses for the LJE's isotope patterns.

A "facies-dependent" model proposes that extremely ^{13}C-enriched carbonates between 2.3 and 2.0 Ga represent localized accentuations of a more moderate global excursion (Schidlowski et al., 1976; Melezhik et al., 1999; Prave et al., 2022). Surveys investigating thousands of carbonates indicate that $\delta^{13}C$ in deeper, open marine waters only increased by +1.5 ‰ during the LJE, while intertidal zones and sabkhas increased by +8 ‰ (Prave et al., 2022; Hodgskiss et al., 2023). Restricted, evaporative marine environments around the globe contain especially elevated $\delta^{13}C$ during the LJE, diminishing with facies shifts to deeper zones (Melezhik et al., 1999; Prave et al., 2022). In modern shallow environments, $\delta^{13}C$ increases because light ^{12}C is removed by enhanced primary productivity, compounded inside relatively restricted water bodies (Aharon et al., 1977; Schidlowski et al., 1985; Swart et al., 2009; Geyman & Maloof, 2019). Experimental data indicates that ^{12}C via CO_2 evaporation can produce carbonates up to +30 ‰, but such values are rarely seen even in modern sabkhas (Stiller et al., 1985; Horton et al., 2016).

The facies-dependent model also has unresolved issues. If the LJE were only driven by localized conditions, it would not stand out as the largest, longest positive $\delta^{13}C$ excursion in Earth history. For example, several $\delta^{13}C$-enriched deposits contain no evidence for restriction (Bekker and Eriksson, 2003; Planavsky et al., 2012), though some can be explained by sediment transport from shallower waters (Prave et al., 2022). Taking both models in perspective, the LJE was likely affected by increasing organic carbon burial and by the growth of shallow, restricted water bodies along continental margins, among other factors. Understanding global vs. local influences on LJE isotopes therefore requires research on more Paleoproterozoic environments and the changes they

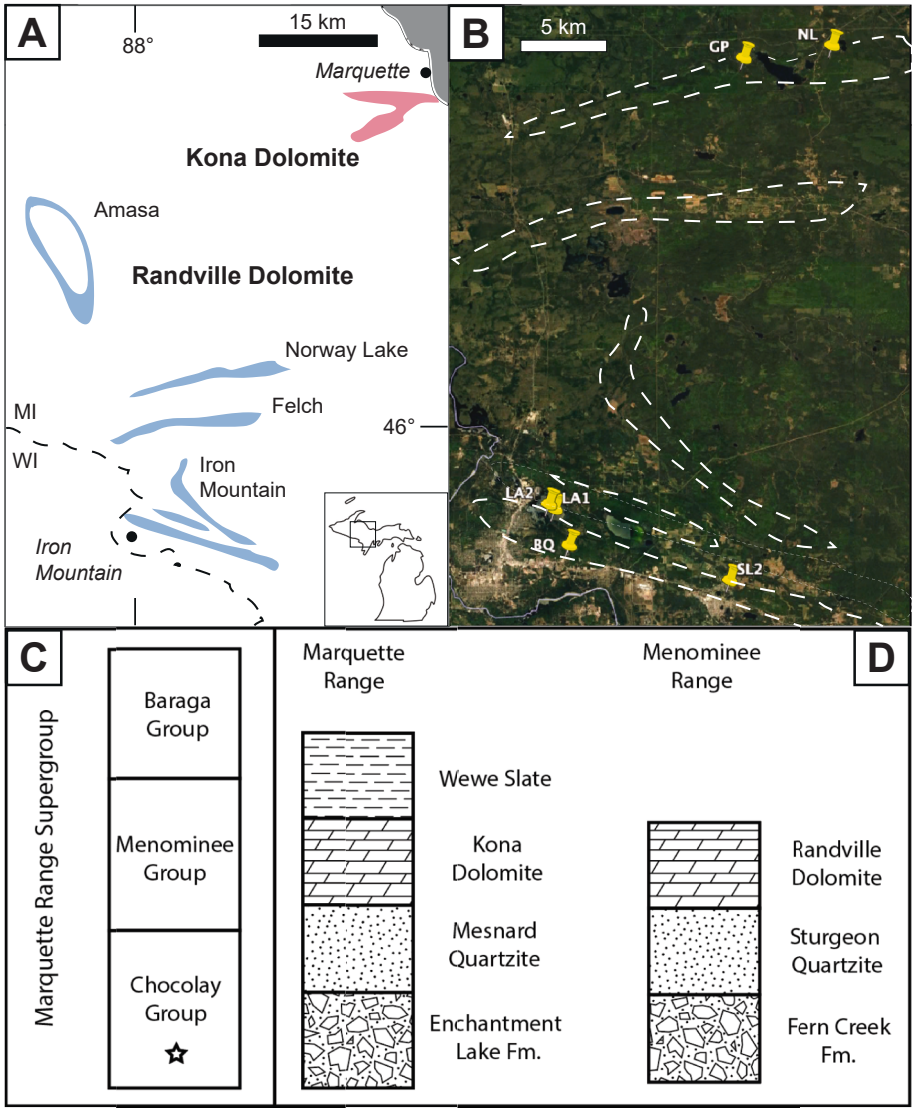

Fig. 1. Location of the Randville Dolomite. A: Major locations of the Randville and Kona Dolomite. B: Sampling locations from this study, with Randville-bearing areas highlighted. NL = Norway Lake, GP = Gene Pond, LA = Lake Antoine, BQ = Bacco Quarry, SL = Strawberry Lake. C: Stratigraphy of the Marquette Range Supergroup.

experienced, especially locations that lack positive carbon isotope excursions.

The Lake Superior region contains several dolomites deposited between 2.4 and 2.0 Ga, with widely varying isotopic compositions (Bekker et al., 2006). The Kona Dolomite near Marquette, Michigan has received the most sedimentary and geochemical research (Fig. 1A) (Twenhofel, 1919; Gair & Thaden 1968; Taylor, 1972; Puffett 1974; Gair 1975; Wohlabaugh and Mancuso, 1990; Bekker et al., 2006). Kona facies broadly represent an evaporative intertidal zone (Taylor, 1972) and contain elevated $\delta^{13}C$ values (+5–10 ‰) typical for many shallow LJE carbonates (Bekker et al., 2006). In contrast, most Paleoproterozoic dolomites in the Lake Superior region have $\delta^{13}C$ values ~0 ‰ (Bekker et al., 2006), average for marine carbonates for most of Earth's history but relatively depleted for LJE deposits. The environmental settings for these "depleted" Superior carbonates are less well-understood than Kona deposits, despite their unique geochemical signatures.

For example, the Randville Dolomite is the next most extensive LJE carbonate in the region but is less well-studied due to increasingly limited exposure (Fig. 1) (Clements & Smyth, 1899; Richardson, 1949; Greenman, 1951; James et al., 1961; Bayley et al., 1966). Previous studies broadly correlated Randville and Kona deposits, but more recent Randville analyses measured average $\delta^{13}C$ values ~0 ‰, much lower than the Kona Dolomite (Bekker et al., 2006). This study addresses the question of local vs. global LJE signals by examining the Randville Dolomite for depositional features that explain "depleted" $\delta^{13}C$ values. The study presents new sedimentology and petrography of Randville sediments and stromatolites, and new isotope datasets to compare with previous studies of Randville, Kona, and other LJE carbonates.

2. Geologic setting

2.1. Supergroup stratigraphy and age constraints

The Randville Dolomite is part of the Paleoproterozoic Marquette Range Supergroup (Fig. 1) (Cannon & Gair, 1970). Marquette Range Supergroup deposits occur throughout the western Upper Peninsula of Michigan and northern Wisconsin, USA, divided into the Chocolay, Menominee, and Baraga Groups. These groups indicate rising sea levels, from shallow dolomites and sandstones (Chocolay Group) to deeper iron formations and shale (Menominee and Baraga Groups). The Chocolay Group is exposed in two regions of the Upper Peninsula (Fig. 1A): the Menominee Range to the southwest near the town of Iron Mountain, and the Marquette Range near Marquette to the northeast (Larue, 1981). Within the Menominee Range, the Chocolay Group consists of three formations (Fig. 1C): the Fern Creek Formation, Sturgeon Quartzite, and Randville Dolomite (Pettijohn, 1943; Larue, 1981). The Fern Creek Formation is characterized by conglomerates followed by rising sea levels to a more sandy coastal environment during the Sturgeon Quartzite (Ojakangas et al., 2001). The Randville Dolomite represents continuing sea level rise into shallow marine waters. Chocolay stratigraphy in the Menominee Range is broadly comparable to the more well-studied Marquette Range to the north (Fig. 1C), where Enchantment Lake Formation conglomerates progress into the Mesnard Quartzite and the Kona Dolomite, ending in the Wewe Slate (Gair & Thaden, 1968; Larue, 1981). A potential Wewe Slate correlate is locally exposed above the Randville Dolomite, but lacks a formal name (Bayley, 1959).

The similarities between Chocolay stratigraphy in the Menominee and Marquette Ranges (Fig. 1C) have led to previous correlations between the Randville and Kona Dolomites, respectively (Richardson, 1949; Greenman, 1951; Bayley et al., 1966; Gair & Thaden, 1968; Young, 1983; Ojakangas et al., 2001). However, it remains unknown whether Randville deposition occurred before, during, or after the more well-dated Kona Dolomite (Fig. 2). The formations are either approximately coeval or represent separate ages in the same broad transgressive cycle (Bekker et al., 2006). The Kona Dolomite's maximum age constraint is 2317 ± 6 Ma, from detrital zircons in underlying

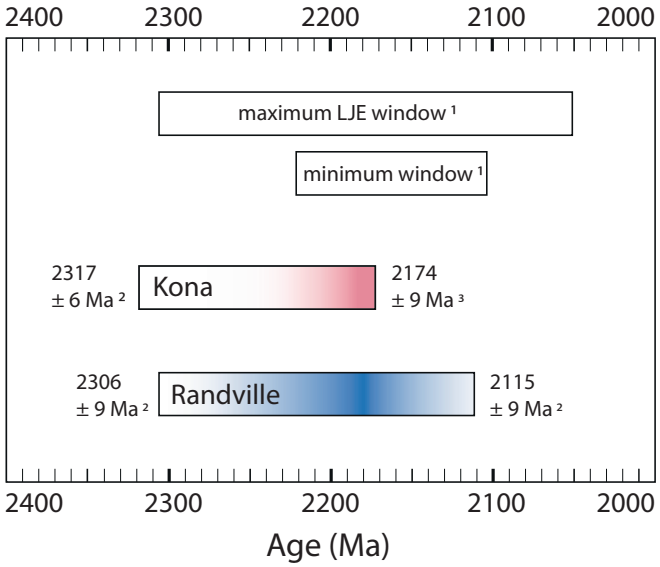

Fig. 2. Age constraints for the LJE, Kona, and Randville Dolomite. Color bars indicate the relative likelihood of deposition based on dating techniques and stratigraphy. References: 1: Martin et al., 2013, 2: Vallini et al., 2006; 3: Rasmussen et al., 2024.

Enchantment Lake Formation (Fig. 2) (Vallini et al., 2006). Until recently, a tentative minimum constraint (2131 ± 13 Ma) was estimated from xenotime overgrowths, also in the Enchantment Lake Formation (Vallini et al., 2006). The xenotime crystals were interpreted as hydrothermal or metamorphic growth after burial of the Chocolay Group, likely related to ~2.2–2.1 Ga mafic dyke formation in the Superior Craton (Buchan et al., 1996; Vallini et al., 2006). Within this ~200 million year window, the Kona Dolomite was previously correlated with the >2.2 Ga Gordon Lake Formation in Ontario based on $\delta^{13}C$ similarities (Bekker et al., 2006). However, Rasmussen et al., 2024 provide a new minimum Kona constraint of 2174 ± 9 Ma from basal tuffs in the conformable, immediately overlying Wewe Slate (Fig. 2). The proximity of these tuffs to the uppermost Kona strongly suggests an age closer to 2174 than 2317 Ma.

The Randville Dolomite's age is less well-defined (Fig. 2). Similar to previous Kona Dolomite age estimates, the Randville's maximum (2306 ± 9 Ma) and tentatively minimum constraints (2115 ± 5 Ma) come from the underlying Sturgeon Quartzite, in detrital zircons and metamorphic xenotime respectively (Vallini et al., 2006). The true minimum constraint for Randville deposits comes from the overlying Menominee Group (1874 ± 9 Ma), separated by a major unconformity (Schneider et al., 2002). This study interprets the 2115 Ma metamorphic xenotime age in conformably underlying quartzites as closer to Randville deposition than the unconformably overlying 1874 Ma age (Fig. 2). The Randville Dolomite experienced similar patterns of metamorphism as underlying quartzites (James et al., 1961; Vallini et al., 2006), and xenotimes below the neighboring Kona Dolomite correlate well with new minimum ages provided from overlying zircons (Vallini et al., 2006; Rasmussen et al., 2024).

Bekker et al., 2006 proposed that the Randville Dolomite is younger than the Kona Dolomite, based on westward-shallowing Kona facies and the southwestward position of Randville deposits (Fig. 1A). However, cross-bedding in each region does not support a direct southwestern transgression from Kona into Randville basins. Paleocurrents in the neighboring basins traveled to the east/southeast along basin axes (Trow 1948; Pettijohn 1957; Larue 1981), with mean-current azimuths at 97.5 degrees in the Marquette Basin (Kona Dolomite, eastward flow) and 143 degrees in the Menominee Basin (Randville Dolomite, flow to the southeast). An analogous coastline would be the adjacent Chesapeake and Delaware Bays on the Atlantic Coast of North America: the

basin axes have similar angles, but transgression would not progress directly from one basin into the other.

In the absence of direct ages, this study conservatively places the end of Randville deposition alongside the end of Kona deposition (2174 Ma), with the potential for a much earlier (<2306 Ma) or later age (>2115 Ma) (Vallini et al., 2006). The implications of age on Randville $\delta^{13}C$ values and the LJE are discussed in Section 5.3.2.

2.2. Localities

The Randville Dolomite's maximum thickness is estimated around 500 m, but individual exposures are rarely over 10 m high and are scattered across areas of intense tree cover. Direct contacts with underlying Sturgeon Quartzite and Archean granites, as well as overlying slates, are rarely observed. Contact with Archean granites is more common in western exposures such as the Amasa Uplift (Fig. 1), potentially representing transgression onto western highlands (Greenman, 1951). The Randville Dolomite lacks a unified stratigraphy, in contrast with the 12 defined members of the Kona Dolomite (Taylor, 1972; Wohlabaugh and Mancuso, 1990; Bekker et al., 2006). James et al. (1961) divided the area near Norway Lake into lower and upper dolomite members divided by a slate with magnetic anomalies, but these results have not been replicated. The majority of Randville studies were performed before 1970, and previously examined outcrops are

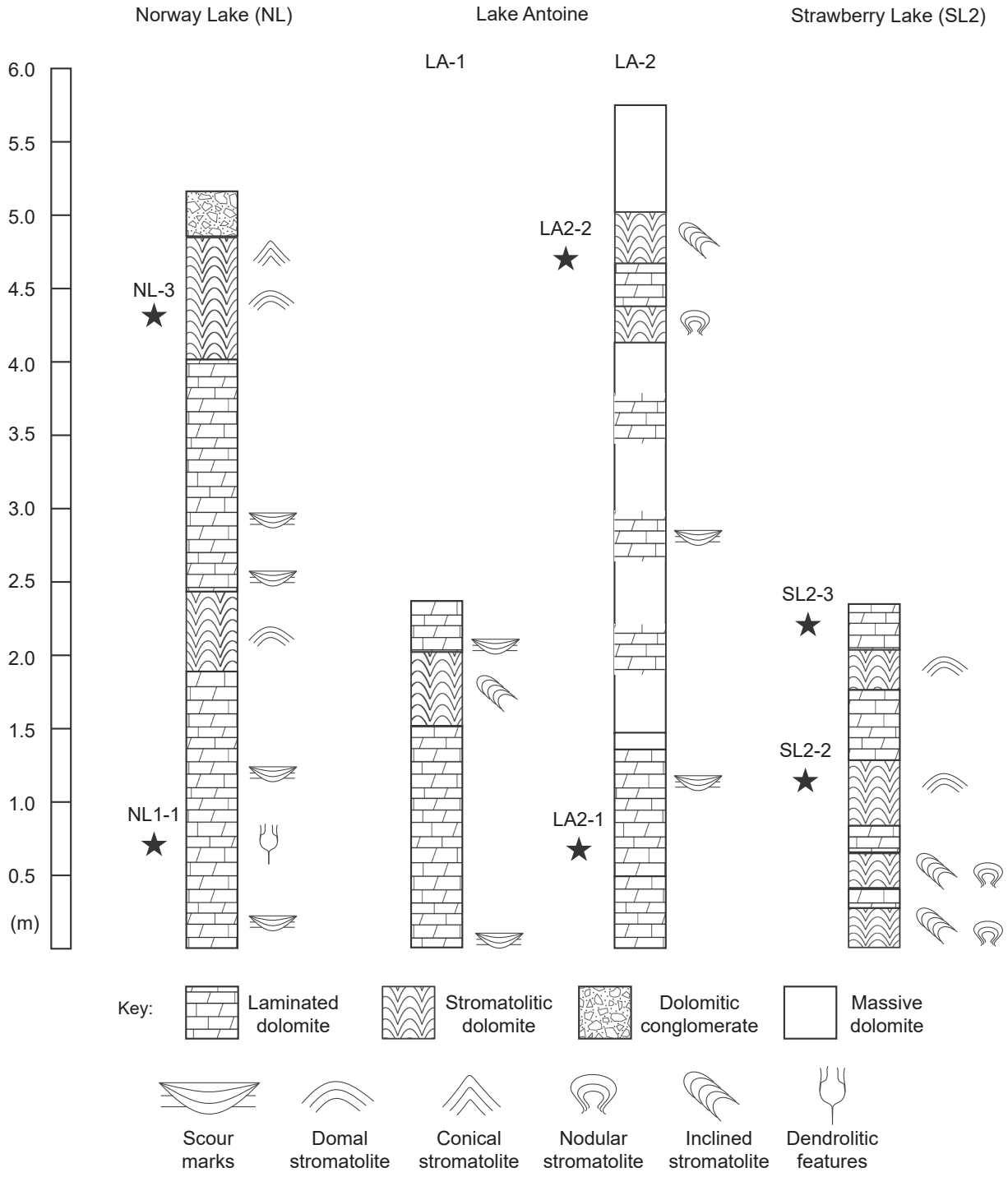

Fig. 3. Stratigraphic columns of the Randville localities studied, with sedimentary structures and stromatolites observed in each.

frequently overgrown or destroyed by construction and quarrying. Despite limited exposure, the Randville Dolomite's wide lateral range and broad correlation with gypsum-bearing marine deposits in the Kona Dolomite have led to interpretations as a shallow, coastal marine environment (Greenman, 1951; Gair & Weir, 1956; James et al., 1961; Bayley et al., 1966).

The Randville Dolomite has four major areas of exposures: Amasa, Norway Lake, Felch, and Iron Mountain from north to south (Fig. 1A, B). This study examines well-preserved sedimentary textures and stromatolites found near Norway Lake and Iron Mountain (Richardson, 1949; Greenman, 1951; James et al., 1961; Bayley et al., 1966). Iron Mountain has the largest Randville exposures, divided into three NW-SE trending belts (Fig. 1A, B). Of these three belts, the southern is most well-exposed and the only unit with described stromatolites (Greenman, 1951; Bayley et al., 1966). The Amasa area (including the Michigamme and Fence River localities) was not examined in this study but also contains sedimentary structures such as oolites, though no stromatolites have been described (Clements & Smyth, 1899; Greenman, 1951; Gair & Weir, 1956). Carbonates in the Felch area have been altered into tremolitic marble and do not preserve primary features (Richardson, 1949; Greenman, 1951; Dryden, 1962). Many Randville Dolomite exposures have been metamorphosed to at least greenschist facies, with rocks in the Felch area experiencing amphibolite-grade or higher alteration (James, 1955).

3. Methods

Samples were collected around Iron Mountain and Norway Lake in Michigan's Upper Peninsula (Fig. 1B). Stratigraphic columns were made at four localities (Fig. 3: NL, LA1, LA2, SL2). Norway Lake (NL) is located ~30 km northeast of Iron Mountain (N 46° 04.3992′ W 87° 49.3197′), in a separate belt of exposure. Two locations in Iron Mountain were sampled near Lake Antoine, one near the south shore (LA1, N 45° 49.8278′ W 88° 01.8454′), and one nearby Eagle Island (LA2, N 45° 49.9829′ W 88° 02.1001′). LA1 is an isolated outcrop two meters tall and roughly 20 by 10 m wide with tilted beds exposed on the top surface, formerly part of a quarry. The orientation of LA1 bedding and stromatolites matches in-situ deposits 400 m to the northwest (LA2), and are also considered in-situ by many studies (Richardson, 1949; Greenman, 1951; Nordeng, 1963; Bayley et al., 1966). LA2 was freshly exposed during construction on Eagle Island in summer 2023. The locality is likely unavailable for further investigation due to housing development, but shows promise for further investigations around Lake Antoine. Strawberry Lake Park (SL2, N 45° 47.5757′ W 87° 53.9444′) was an exposed hilltop section in Norway, Michigan, 14 miles east of Iron Mountain. A quarry in Iron Mountain (Bacco Quarry, BQ, N 45° 48.6895′ W 88° 01.1869′) contained abundant stromatolitic float, while an isolated boulder exposure near Norway Lake contained a well-preserved conglomerate bed (Gene Pond, GP, N 46° 03.9934′ W 87° 53.3240′).

Two rock samples were selected from Norway Lake (NL, three powders each), Lake Antoine (LA2, five powders each), and Strawberry Lake (SL2, five powders each) (Fig. 3). From Norway Lake, sample NL1-1 was from a planar-laminated dolomite with mm-scale dendrolitic microstructures, while sample NL-3 was from domal stromatolitic layers near the section's top. From Lake Antoine, sample LA2-1 came from planar laminated dolomite, while sample LA2-2 was from layers of an inclined stromatolite. From Strawberry Lake, sample SL2-2 was from a domal stromatolite, while sample SL2-3 was from planar laminated dolomite at the top of the section. Each hand sample was between five and fifteen cm in diameter. Points were drilled using a diamond burr-tipped Dremel rotary tool near thin section sites, avoiding areas with extensive fractures or recrystallization. Points were drilled with ~0.5 cm distance in between each layer sampled.

Samples were cut using water-cooled saws to select areas for thin-section analysis. Petrography was analyzed using an Olympus BX-51 microscope with a Jenoptik camera with mosaic software to combine multiple photographs into larger images. Powders (n = 26) were collected for $\delta^{13}C$, $\delta^{18}O$, and Mn/Sr analyses. Powder samples (~0.001 g) were analyzed at the University of Michigan, Ann Arbor, using a ThermoFisher MAT253 mass spectrometer with a Kiel IV automated preparation device to quantify $\delta^{13}C$ and $\delta^{18}O$ abundance. To quantify manganese/strontium ratios, $\delta^{13}C$ and $\delta^{18}O$ powder sample sites were redrilled, collecting ~0.01 g using a Dremel diamond burr. A calibration curve was set in a 10 mL solution of 2 % Nitric Acid using diluted Mn and Sr standards. Diluted samples were run on an Agilent 5800 ICP-OES with a Varian SpectrAA 200 Atomic Absorption Spectrometer.

4. Results

4.1. Stratigraphy

At the studied localities, the Randville Dolomite is broadly divided into three facies: stromatolitic, laminated, and conglomerate (Fig. 3).

4.1.1. Stromatolites

Stromatolites were present in all measured outcrops, exhibiting a range of morphologies including domal, nodular, conical, and inclined forms.

4.1.1.1. Domal. Domal stromatolites are found in Norway Lake (NL), and at the SL2 and BQ localities in Iron Mountain (Fig. 4). Domal stromatolites at NL are up to 6 cm wide and 3 cm high (Fig. 4A), with fine layers 1–3 mm thick. When stratigraphic contacts are visible, NL domes are underlain and succeeded by laminated dolomites (Fig. 4A). Strawberry Lake (SL2) domes are much larger, between 20 and 30 cm wide and 10–25 cm high (Fig. 4B). Onlapping of surrounding sediments and crinkled internal layering distinguish these wider stromatolites from cross-beds seen elsewhere in Randville deposits. Layering is less distinct due to recrystallization and silicification, with chert layers measuring 1–2 cm and the dolomite layers 2–3 cm (Fig. 4B).

In BQ, domes are only observed in loose boulders removed during quarrying (Fig. 4C, D), with no stromatolites observed on the remaining rock faces. BQ domes are 10 cm wide by 10 cm high. Layers are smooth, 0.2–1 cm thick, and have relief up to 5 cm from their bases (Fig. 4C). Bedding planes reveal ellipsoidal cross-sections with thin, concentric layering, separated by 1–2 cm of dark chert (Fig. 4D). In plan view, outer stromatolite margins are irregular, cross-cutting through several concentric layers (Fig. 4D). In some places, immediately adjacent stromatolites appear to nucleate from these erosive margins, forming incomplete ellipsoids (Fig. 4D).

4.1.1.2. Nodular. Nodular stromatolites have roughly equal heights and widths (Fig. 5A, B), with diameters expanding from narrow bases into wider mid-sections and rounded tops (Grey & Awramik 2020). As nodular stromatolites flare outward, their sides are typically oversteepened beyond 90 degrees from bedding. Similar terms for stromatolites with bases narrower than their maximum width include "bulbous" and "turbinate", which are typically taller than wide (Grey & Awramik 2020). Nodular stromatolites are distinct but rare, with only three individual structures found in Iron Mountain: one at LA2 (Fig. 5A) and two at SL2 (Fig. 5B), always in association with inclined stromatolites. The LA2 sample is the largest and most well-defined nodular structure (Fig. 5A), 6 cm wide by 4 cm tall. Layers within the stromatolite have variable thickness between 1 and 5 mm. The lone stromatolite rises sharply from planar, thinly-bedded dolomite below, while the top gently grades back into overlying planar beds. Layers laterally adjacent to the stromatolite are highly silicified (Fig. 5A). In contrast, the stromatolite itself is mostly tan dolomite with minor brown layers of chert, save for a chert-rich core. An inclined stromatolite rises from the same bedding plane ~10 cm to the left (Fig. 6C) but does not merge or interact with the nodular stromatolite.

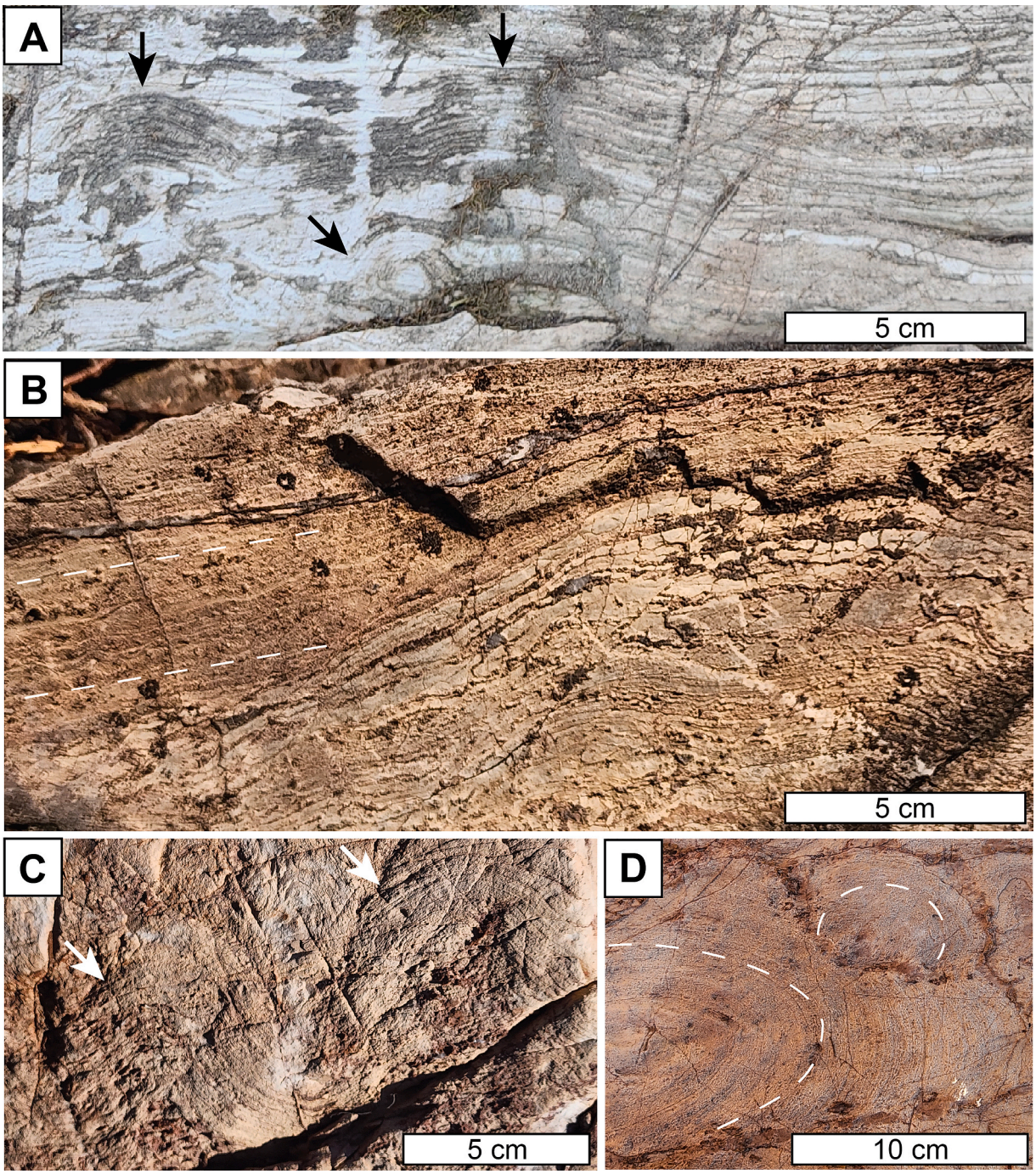

Fig. 4. Domal Randville stromatolites. A. Norway Lake (NL), cross-section, 2.0 m from base. Arrows note individual heads. Tan coloration on the right is due to surficial weathering, while paler layering on the left is due to fresh exposure. B: Bacco Quarry (BQ), plan view, float. Stromatolite heads are separated by thin rinds of chert and interstitial sediment. The outer edge of the larger sample is erosional, cutting through several generations of layers. The smaller stromatolite on the margin nucleates from this erosional margin. C: Bacco Quarry (BQ), cross-section, float. Arrows note individual heads. D: Strawberry Lake (SL2), cross-section, 2.0 m from base. Dashed lines indicate onlapping sediments on the left-hand margin. Darker layers are more highly silicified.

In contrast, the two nodular stromatolites in SL2 are not isolated structures but early stages of growth for later inclined stromatolites (Fig. 5B). The SL2 stromatolites are found in light gray, unsilicified dolomite, and are half the size of the LA2 sample (2.5 cm wide by 1.5 cm tall) (Fig. 5B). Their bases and mid-sections are closer in diameter, approaching domal morphologies. Both stromatolites are found near the base of LA2 stratigraphy. One rises from slightly wavy laminated dolomite (Fig. 5B), while the base of the other is obscured. Both structures directly transition into inclined stromatolites which continue for ~40 cm of stratigraphy (Fig. 5B, 6D) before replacement by laminated dolomite (Fig. 6E).

4.1.1.3. Conical. Only one potentially conical stromatolite was observed (Fig. 5C), near the top of the Norway Lake section (NL). The cone was 20 cm wide by 15 cm tall. Layers in this sample were much thicker than other Norway Lake structures, between 0.2 and 0.5 cm high, alternating between white dolomite and pink chert (Fig. 5C). The cone starts in slightly contorted laminated dolomite, and rises through a domal morphology into a broad, slightly inclined cone. The structure is heavily fractured, missing upper and lateral contacts that would

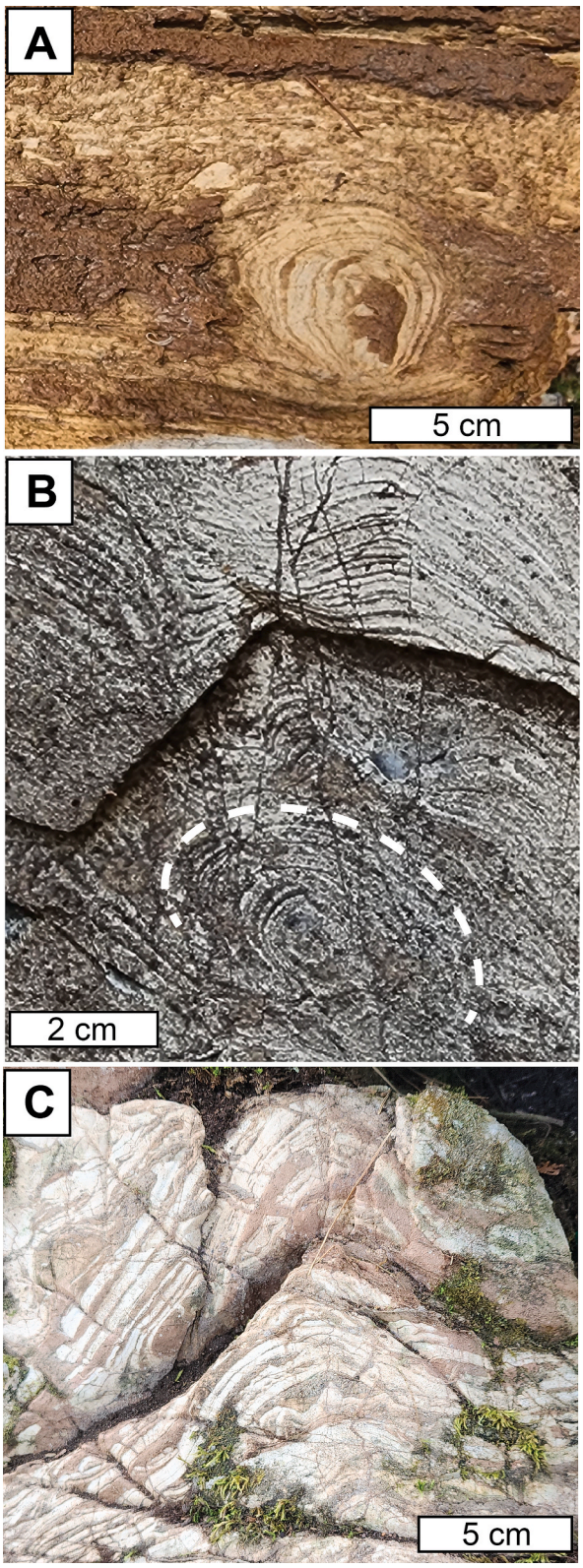

Fig. 5. Nodular & conical Randville stromatolites. All images are in cross-section. A: Nodular stromatolite, Lake Antoine (LA-2), 4.2 m from base. Note onlap of darker, silicified sediment layers on either side of the stromatolite. B: Nodular stromatolite, Strawberry Lake (SL-2), 0.5 m from base. The nodular sample grades upward into inclined stromatolites (see Fig. 6). C: Conical stromatolite, Norway Lake (NL), 4.7 m from base.

demonstrate sediment onlap (Fig. 5C) and has the potential to represent soft-sediment deformation such as a slump-induced fold instead of a microbial deposit.

4.1.1.4. Inclined. Inclined stromatolites (Fig. 6) were observed in Iron Mountain localities (LA1, LA2, SL2), but not in Norway Lake. In LA1, tan stromatolites form climbing domes 10–20 cm wide (Fig. 6A, B). Layers are smooth and vary between 0.5 and 2 cm thick, thicker than other stromatolites around Lake Antoine. The relief of individual layers is low, with heights ≤3 cm from their bases. Individual LA1 stromatolites sit immediately adjacent to each other with no interstitial sediment, but are not laterally linked (Fig. 6A, B). Instead, stromatolite margins are ragged, with successive layers widening and narrowing by up to a centimeter (Fig. 6B), infringing on the growth of neighboring domes. Layering in adjacent stromatolites is not identical but shares similar patterns of thickness (Fig. 6A). LA1 stromatolites nucleate from a wavy unconformity overlying laminated and cross-bedded dolomite of similar bed thickness and composition (Fig. 6A). After 30 cm, stromatolite layers gradually transition upward into scour-fill structures, then laminated dolomite, with layers thinning to sub-cm scales (Fig. 6A). The angle of growth shifts from ~60 degrees (from vertical) to vertical (perpendicular to bedding planes) over stromatolite growth. Apart from structure and bed thickness, the composition of dolomite remains similar throughout, with little to no silicification evident.

Inclined stromatolites are also present 400 m away in LA2, but express different morphologies (Fig. 6C). LA2 stromatolites occur as isolated, narrow columns surrounded by laminated dolomite. Columns are 2 cm wide, remaining relatively constant throughout growth. The LA2 stromatolites grow at more extreme angles than LA1, consistently ~60 degrees from vertical (Fig. 6C). Stromatolite growth gradually arises from and terminates into laminated dolomite, 50 cm along inclination across 20 cm of vertical stratigraphy (Fig. 6C). The column margins also merge seamlessly into adjacent laminated dolomite layers, with no ragged edges (Fig. 6C). Layer thickness matches surrounding laminations, between 1 and 3 mm thick. LA1 samples are slightly more silicified, usually along individual laminations.

Stromatolites in SL2 present another distinct inclined morphology (Fig. 6D, E). The stromatolites' internal layering broadly resembles LA2 textures, composed of smooth laminations 1–3 mm thick that merge with adjacent laminated dolomite. In contrast, the larger structures of SL2 stromatolites form many wavy domes and columns (Fig. 6D), rather than the isolated features of LA2. Stromatolites are laterally-linked and immediately adjacent, with no room for interstitial sediment. The width and shape of SL2 stromatolites is variable, shifting from broader domes to narrower columns 1–3 cm wide (Fig. 6D). Growth angles shift between 20 and 50 degrees from vertical. Lower boundaries are obscured at the bottom of the section, but stromatolites gradually flatten into laminated dolomite (Fig. 6E).

4.1.2. Laminated Dolomite

Laminated dolomite occurs in all localities, and is especially abundant near Norway Lake and Lake Antoine (Fig. 7A-D). Bedding is typically planar, with individual layers ranging between 0.5 and 4 cm thick, typically ~1 cm (Fig. 7D). In many beds, dolomite layers are interspersed with minor chert layers, 0.2–2 cm thick. Primary features are more visible in weathered surfaces, which vary in color between localities. Norway Lake dolomites include alternating white and pale pink layers, Lake Antoine and Bacco Quarry outcrops are usually tan to brown, while individual Strawberry Lake beds shift from black, pale gray, and beige.

Evidence for occasional disturbances occur in Norway Lake and Lake Antoine deposits. Rare, isolated scour-fill structures are typically 20 cm wide and 4 cm deep (Fig. 7A and B). In Norway Lake, planar layers transition into oversteepened, buckled fragments (Fig. 7C). Recrystallization obscures a precise identification, but such features potentially

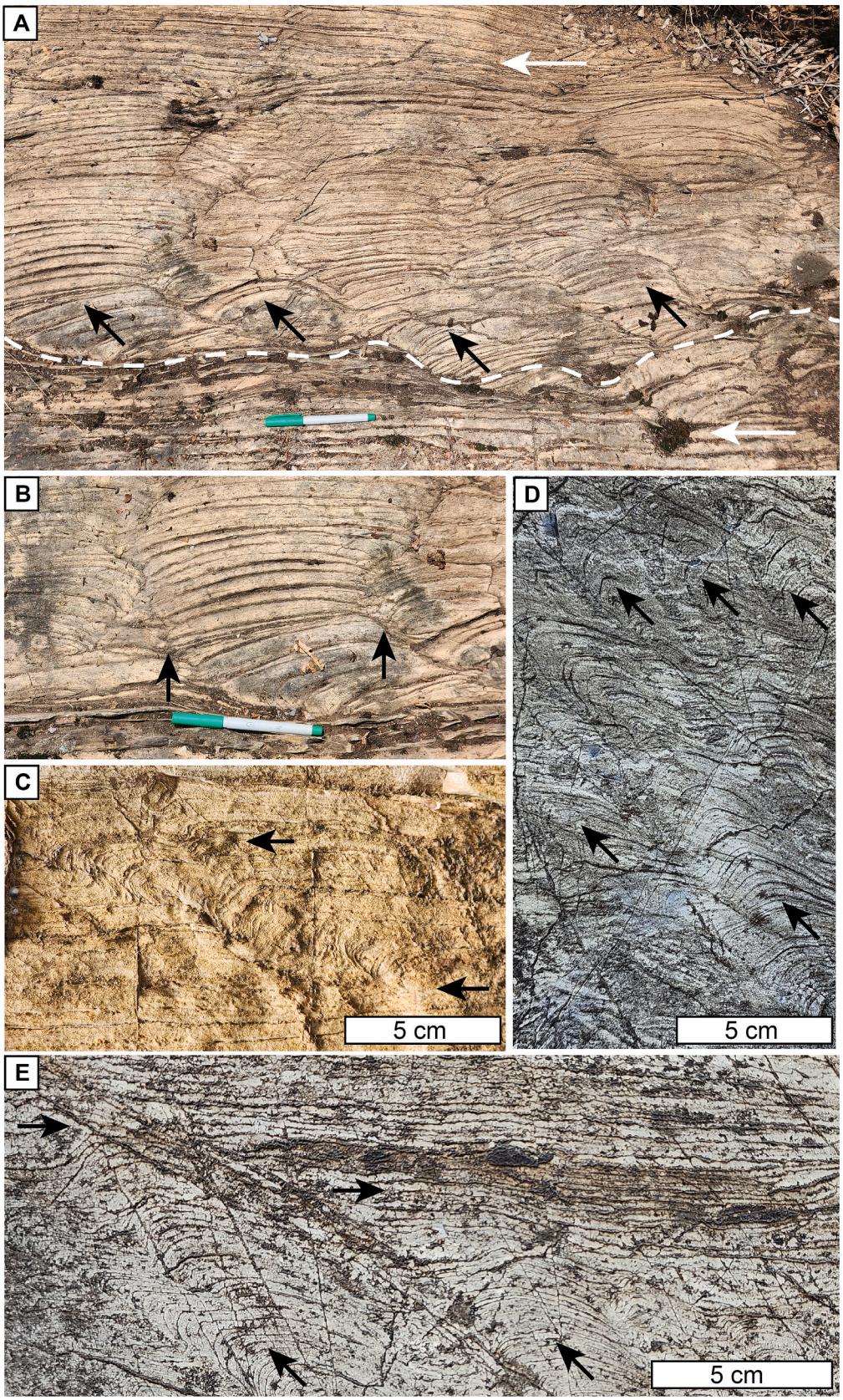

Fig. 6. Inclined Randville stromatolites. All images are in cross-section. A: Lake Antoine (LA1), 2.0 m from base. Pen is 15 cm for scale. Stromatolites initially grow between 45 and 60 degrees (black arrows) from an erosional surface (dashed line), shifting to vertical growth. Horizontal lines indicate planar bedding before and after stromatolite growth. B: Same location as A. Three adjacent stromatolites, with back arrows noting "ragged" margins" of irregular width. C: Lake Antoine (LA2), 4.7 m from base. Arrows note the start and termination layers of the stromatolite. Note the lateral persistence of layers from the stromatolite into adjacent planar

dolomite. D: Strawberry Lake (SL2), 0.5 m from base. Arrows note individual stromatolite heads. E: Same location as D. Horizontal arrows note the transition from stromatolites to planar beds.

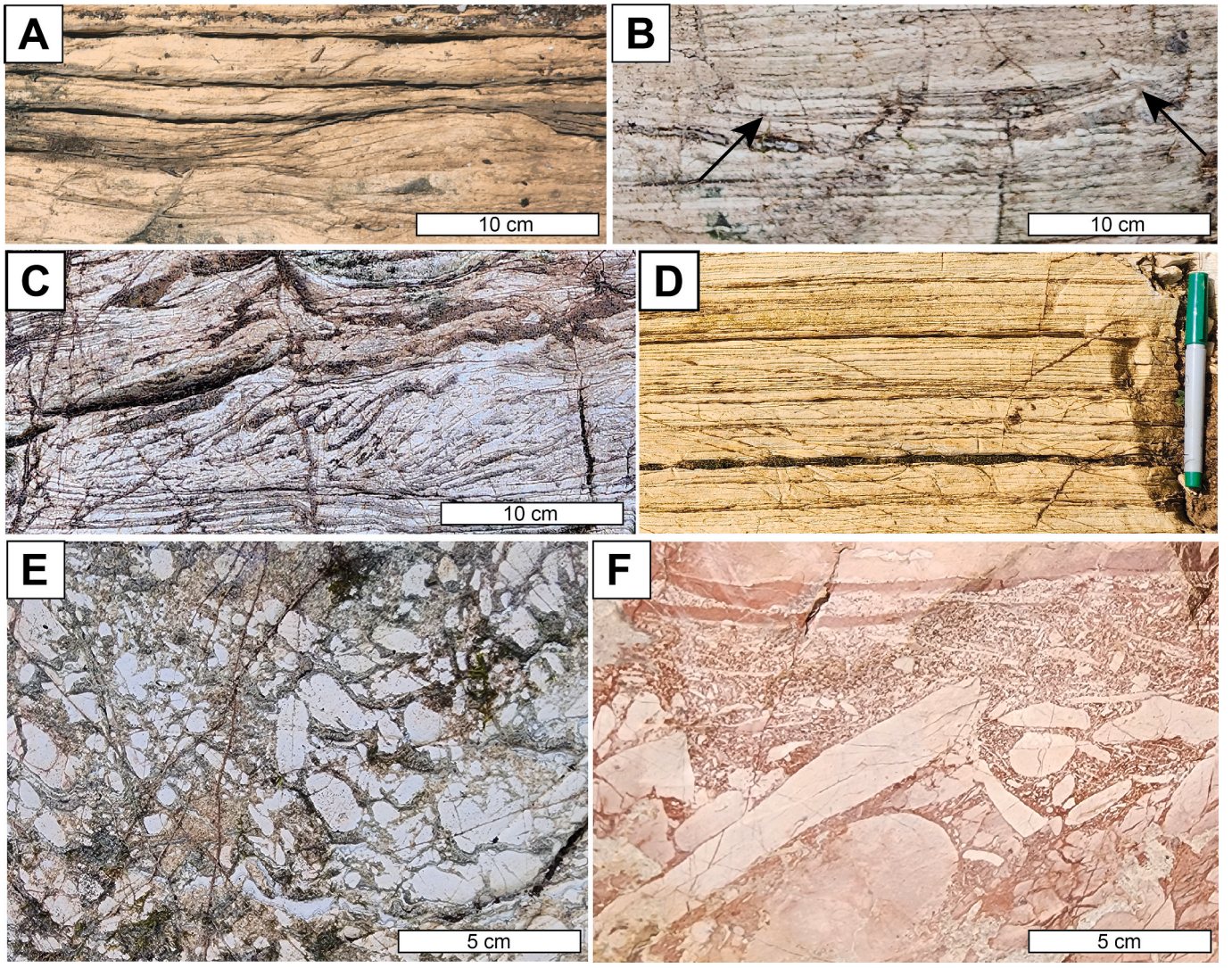

Fig. 7. Sedimentary structures. All images are in cross-section. A: Lake Antoine (LA1), base of section, scour mark, B: Norway Lake (NL), 1.2 m from base, scour mark, C: Norway Lake (NL), 3.0 m from base, slumping and potential soft-sediment deformation, D: Lake Antoine (LA-2), 1.0 m from base, laminated dolomite. Pen is 15 cm for scale. E: Norway Lake (NL), top of section, dolomitic conglomerate, F: Gene Pond (GP), float, dolomitic conglomerate with some elongate clasts.

indicate motion during soft-sediment deformation. Such deformation in Norway Lake broadly decreases up-section (Fig. 7B), grading into stromatolitic and planar-laminated dolomites.

Layering is obscured in freshly exposed faces, most notably in the construction site of LA2. A 2.5-meter section had recently been excavated, and the newly-cut surfaces revealed few traces of lamination. Based on the structures observed and the extent of laminated dolomite around Lake Antoine, this study conservatively assigns this "massive" unit as laminated facies, which we infer would look broadly similar to other localities given time for surficial weathering.

4.1.3. *Dolomitic conglomerate*

Dolomitic conglomerate was only observed in the top unit of Norway Lake (Fig. 7E), and in float at Gene Pond in the same belt of sediment (Figs. 1B, 7F). The Norway Lake bed is 40 cm thick and unconformably overlays stromatolite deposits. Dolomite clasts are poorly sorted, subrounded to subangular, and range between 0.5 and 6 cm in diameter. Clasts are pure white dolomite within a gray matrix of mixed dolomite and chert. The conglomerate's upper surface quickly grades into dolomitic granules before becoming obscured. No other sedimentary structures were observed within the conglomerate. Clasts in the Gene Pond location were also white dolomite, but had a wider variety of sizes from granules to 15 cm long (Fig. 7E). Clast shapes were also more diverse, from long, flat, subangular pieces to subrounded ovals (Fig. 7E). The single conglomerate observed demonstrated roughly graded bedding from cobbles upward to granules and laminated dolomicrite (Fig. 7E). Dolomicrite layers and matrices were various shades of pink in weathered exposures.

4.2. *Microbialite petrography*

4.2.1. *Stromatolites*

Stromatolites contain variable microstructure preservation (Fig. 8A–C). In Strawberry Lake, inclined stromatolites are composed of alternating arched layers of dolomitic micrite and microspar (Fig. 8A and B). Thinner micrite layers tend to be darker and approximately 50

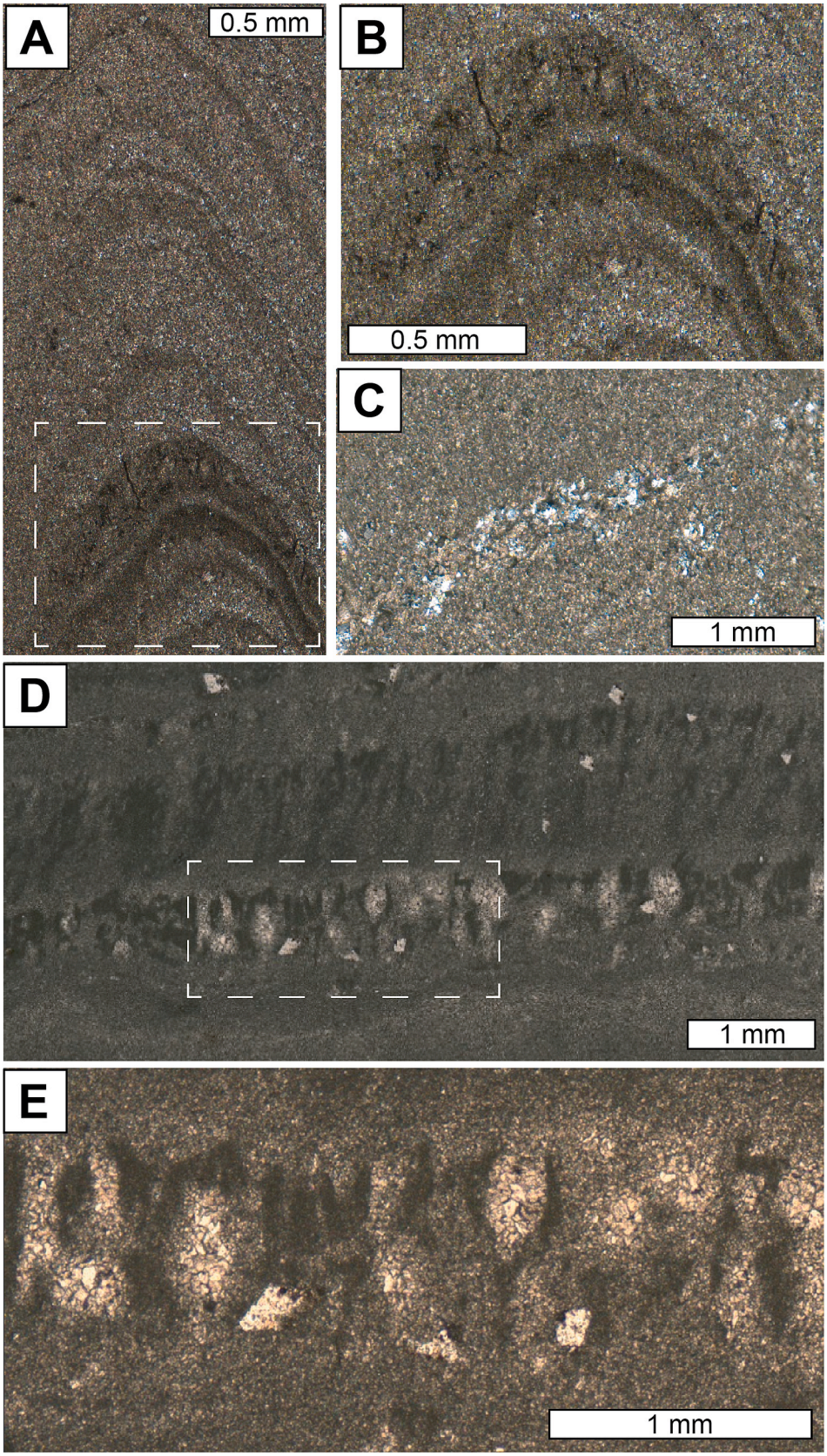

Fig. 8. Microbialite petrography. A: Inclined stromatolite, Strawberry Lake (SL-2). B: Inset from A, with alternating micritic and microspar layers. C: Inclined stromatolite, Lake Antoine (LA-2), with thick cm-scale microspar layers separated by sub-mm chert laminations. D: Multiple "dendrolite" layers, Norway Lake (NL-1). E: Inset from D, highlighting micritic, occasionally branching "dendrolite" filaments separated by spar-filled former voids.

μm thick, while thicker microspar layers are typically around 250 μm (Fig. 8B). Throughout this sample, there are many fractures filled with dark amorphous material, most likely organic matter. In contrast, inclined Lake Antoine stromatolites are less well-preserved (Fig. 8C), with no micrite or organic carbon. Instead, successive layers are composed of featureless microspar layers up to 1.5 cm thick, divided by sparry layers that are 100 μm thick (Fig. 8C). Thin tremolite crystals were observed within Lake Antoine stromatolites but not in Strawberry Lake stromatolites. No clastic grains were observed in any stromatolite thin section.

4.2.2. *Dendrolite-like structures*

A sample of planar laminated dolomite from Norway Lake contains micritic layers up to 2 mm thick (Fig. 8D and E). Micritic layers exhibit dendrolitic patterns: elongated, slightly angled micrite clusters forming branching structures up to 1 mm tall. Voids between the structures are with dolomitic spar (Fig. 8E). Thicker dolomite microspar layers appear above and below the branched structures. No clastic grains were observed in sample NL-1. Sparry dolomite rhombs appear sporadically throughout the sample, cross-cutting through primary fabrics (Fig. 8D and E).

4.2.3. *Rip-up fabrics*

Laminated dolomites in Norway Lake, Strawberry Lake, and potentially Lake Antoine contain rip-up clasts, elongated pieces of dolomitic micrite that range from 100 μm to1 cm in length (Fig. 9). In all three locations, clasts are made of pure dolomicrite. Norway Lake rip-ups are typically blockier (Fig. 9A and B), while Strawberry Lake has long, thin, wavy fragments (Fig. 9C). Irregular void spaces between clasts are filled with dolomitic cements in Norway Lake (Fig. 9A and B) and quartz cements in Lake Antoine (Fig. 9C). In Lake Antoine laminated dolomites

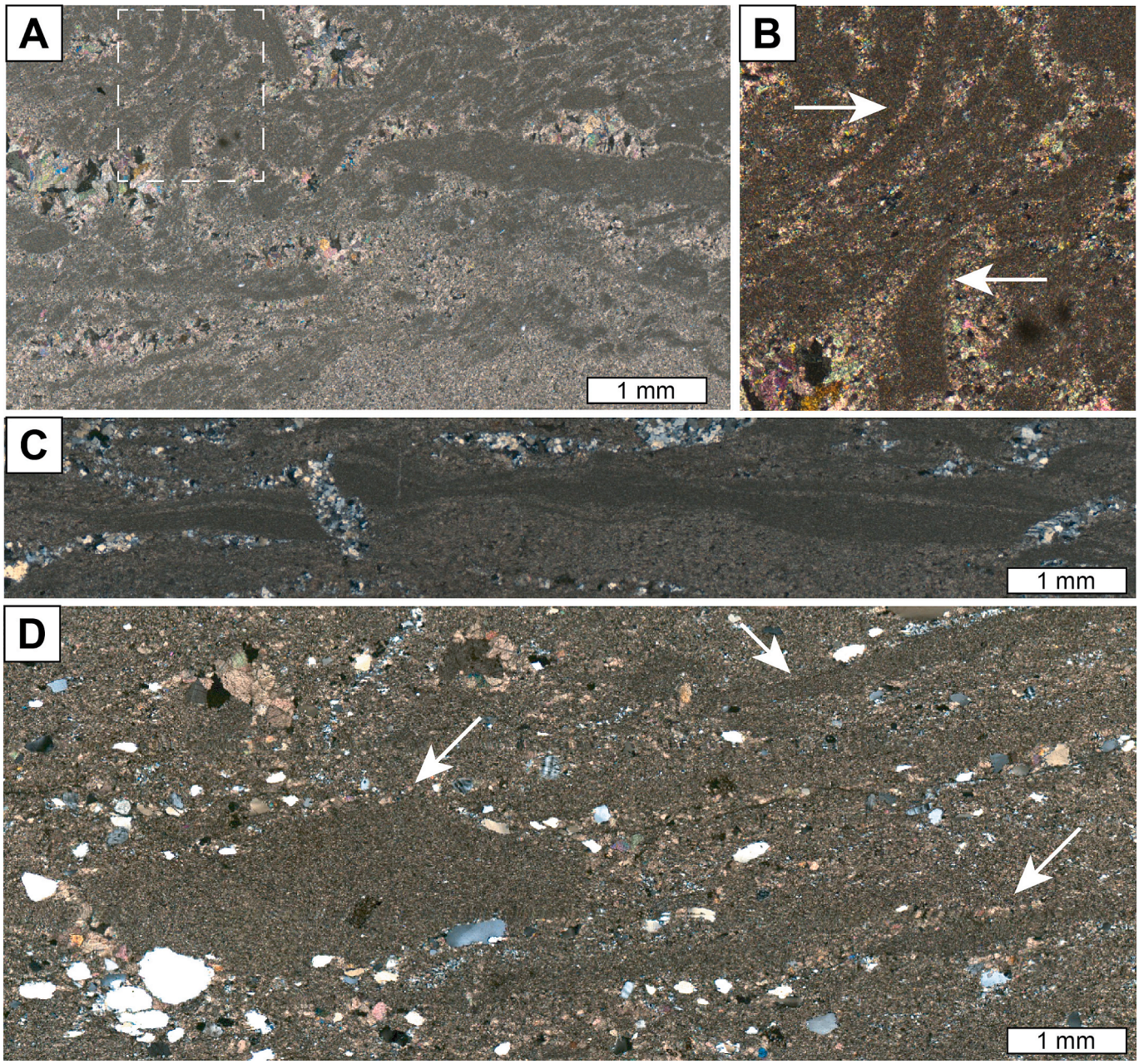

Fig. 9. Petrography of disturbed sediments. A: Norway Lake (NL), abundant sub-mm and mm-scale carbonate clasts, with some exhibiting curved microbial rip-up morphologies. B: Inset of A, noting curved clasts. C: Strawberry Lake (SL2), thin, wispy rip-up structures, C: Lake Antoine (LA2), micritic carbonate clasts (arrows) in a matrix of micrite and clastic sand grains.

(Fig. 9D), with featureless dolomitic microspar interrupted by a 1 cm thick layer of coarse sand grains and micrite clasts (Fig. 9D). However, none of the micrite clasts exhibit irregular wavy or crinkled microbialite textures. The matrix surrounding Lake Antoine dolomite clasts are contain clastic sand grains the only such grains observed in any Randville thin-sections from this study (Fig. 9D).

4.3. Geochemistry

Measured $\delta^{13}C$ values in Randville samples range from 0.51 to 1.68 ‰, with $\delta^{18}O$ between −8.11 and −5.91 ‰ (Fig. 10A, Table 1). There is no correlation between $\delta^{13}C$ and $\delta^{18}O$ in any Randville locality, nor across the entire dataset. Individual locations show slight isotopic variations. Norway Lake (NL) contained the lightest $\delta^{13}C$ (0.51–1.12 ‰) and a relatively wide range of $\delta^{18}O$ (−8.06 ‰ to −5.91 ‰). Strawberry Lake (SL2) had slightly heavier $\delta^{13}C$ (1.1 ‰–1.5 ‰) and more constrained, lighter $\delta^{18}O$ (−8.11 ‰ to −7.15 ‰). Lake Antoine (LA2) contained the most enriched $\delta^{13}C$ (1.32–1.68 ‰), and lighter $\delta^{18}O$ than Strawberry Lake (−7.05 to −6.51 ‰).

Elemental concentrations of Mn and Sr were also measured to provide relative indices of meteoric alteration. Increasing alteration is indicated by enriched Mn and depleted Sr, resulting in higher Mn/Sr concentrations. Across all Randville locations studied, concentrations of Mn ranged from 56 to 614 ppm, with Sr concentrations between 18 and 63 ppm, with Mn/Sr ratios between 0.9 and 31 (Fig. 10B, Table 1). Lake Antoine had the lowest Mn (56 ppm–95 ppm), highest Sr (52 ppm–63 ppm), and Mn/Sr ratios between 0.9 and 1.6. Norway Lake had intermediate Mn (187 ppm–294 ppm), Sr (44 ppm–63 ppm), and Mn/Sr ratios (3–5). Strawberry Lake had the highest Mn (440 ppm–614 ppm), lowest Sr (18 ppm–28 ppm), and highest Mn/Sr ratios (17–31). Overall, there is no correlation between Mn/Sr ratios and isotopic data (Fig. 10B).

5. Discussion

5.1. Depositional environment

The most extensive Randville sedimentology study is an unpublished Master's thesis over seventy years old (Greenman 1951). Many localities investigated by Greenman and USGS surveys (Clements & Smyth 1899; Gair & Weir 1956; James et al., 1961; Bayley et al., 1966) have either been severely reduced by forest overgrowth (NL, SL2) or from construction (LA1, LA2, BQ). For example, Greenman recorded ~60 m ("nearly 200 feet") of exposure at LA1 in 1949, a quarry on the south shore of Lake Antoine at the time. As of summer 2023, the location only contains <5 m of stratigraphy in an isolated, overgrown block. As a result, several previously recorded sedimentary structures were not observed in this study, yet remain crucial to paleoenvironmental interpretations. This discussion of sedimentary features and stromatolites synthesizes our recent measurements with older, unpublished datasets

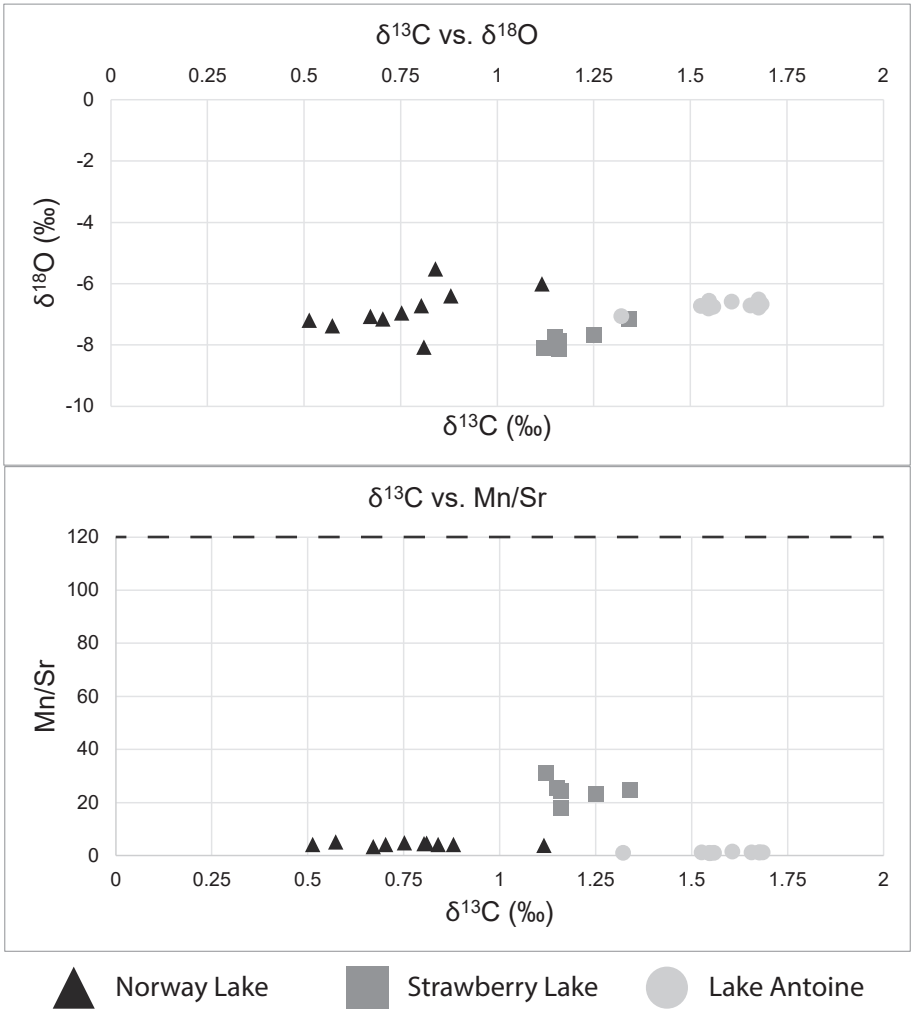

Fig. 10. Randville Dolomite geochemical data. A: $\delta^{13}C$ vs. $\delta^{18}O$, B: $\delta^{13}C$ vs. Mn/Sr. Dashed line = maximum accepted Mn/Sr value for LJE-era carbonates in the Lake Superior region, Bekker et al. (2006). Error bars are smaller than sample markers.

Table 1
Randville Dolomite geochemistry.

Sample	Locality	$\delta^{13}C$ (‰)	$\delta^{18}O$ (‰)	Mn (ppm)	Sr (ppm)	Mn/Sr
LA2-1	Lake Antoine	1.32	−7.05	65.1	55.8	1.17
LA2-1	Lake Antoine	1.61	−6.58	95.8	59.9	1.60
LA2-1	Lake Antoine	1.55	−6.55	59.6	63.2	0.94
LA2-1	Lake Antoine	1.55	−6.80	56.9	52.1	1.09
LA2-1	Lake Antoine	1.56	−6.74	57.6	53.5	1.08
LA2-2	Lake Antoine	1.68	−6.77	67.8	54.2	1.25
LA2-2	Lake Antoine	1.68	−6.66	72.4	58.8	1.23
LA2-2	Lake Antoine	1.53	−6.71	71.4	53.6	1.33
LA2-2	Lake Antoine	1.68	−6.51	71.4	57.1	1.25
LA2-2	Lake Antoine	1.66	−6.70	76.5	61.2	1.25
SL2-2	Strawberry Lake	1.34	−7.15	450.0	18.0	24.98
SL2-2	Strawberry Lake	1.25	−7.66	440.4	18.8	23.45
SL2-2	Strawberry Lake	1.15	−7.72	498.5	19.6	25.43
SL2-3	Strawberry Lake	1.16	−7.87	491.5	20.2	24.28
SL2-3	Strawberry Lake	1.12	−8.10	614.4	19.8	31.03
SL2-3	Strawberry Lake	1.16	−8.11	506.8	28.4	17.84
NL1-1	Norway Lake	0.84	−5.51	187.1	44.2	4.23
NL1-1	Norway Lake	1.12	−6.01	202.4	53.6	3.77
NL1-1	Norway Lake	0.88	−6.40	231.8	56.3	4.11
NL1-1	Norway Lake	0.80	−6.71	248.5	55.0	4.52
NL1-1	Norway Lake	0.81	−8.06	257.1	55.0	4.67
NL3	Norway Lake	0.57	−7.37	294.4	56.5	5.21
NL3	Norway Lake	0.67	−7.06	217.9	63.4	3.44
NL3	Norway Lake	0.70	−7.15	238.1	57.5	4.14
NL3	Norway Lake	0.51	−7.19	239.8	58.0	4.13
NL3	Norway Lake	0.75	−6.96	275.7	56.8	4.86

Values of $\delta^{13}C$, $\delta^{18}O$, Mn, Sr, and Mn/Sr for dolomite samples from Lake Antoine, Strawberry Lake, and Norway Lake.

of more extensive exposures.

5.1.1. Scours and conglomerates

The most abundant facies observed were planar dolomites intermittently punctuated with scouring and intraformational conglomerates, especially in the Lake Antoine and Norway Lake areas (Fig. 7A–D). Scouring is relatively infrequent and small scale (~20 cm wide, ~4 cm deep, Fig. 7A,B). In other carbonate deposits, scouring is observed in low-energy lagoons and distal ramps (Massari & D'Alessandro 2000; Switzer & Jones 2008; Jacquemyn et al., 2018). Such examples are typically several meters in scale, interpreted as tsunami events, while the smaller scale of Randville scours indicate less severe storm events. In thin sections, Greenman (1951) observed a higher degree of clastic sand grains inside disturbed dolomites than laminated beds. The highest abundance of quartz sand was >80 %, but nearly half of the samples investigated had <10 % clastic grains. Regardless of relative depth, many Randville deposits appear to have been deposited in relatively calm environments punctuated by storm events scouring seafloors and introducing clastic sand.

This study only observed conglomerates in northern Randville exposures near Norway Lake and Gene Pond (Figs. 1 and 7). Greenman (1951) described additional exposures around Iron Mountain, including an ~8 m unit near Lake Antoine with frequent conglomerate interbeds, which has since been destroyed. Lake Antoine conglomerates were apparently associated with mud cracks, but the photographic evidence is too exposed to definitively confirm. The Lake Antoine conglomerates were interpreted as exposure, desiccation, and subsequent disturbance of peritidal carbonate seafloors (Greenman, 1951). If so, Lake Antoine would have the only evidence of subaerial exposure in the Randville Dolomite. Greenman noted that no other locality contained mud cracks, and no other study has recorded evidence for evaporative environments.

The term "flat-pebble conglomerates" was initially used to describe Randville beds, based on the presence of flat, elongate clasts (Greenman, 1951). While such clasts were observed near Gene Pond (Fig. 7F), they were associated with dolomitic clasts with various shapes and rounding in a very poorly-sorted conglomerate. Other poorly-sorted dolomitic conglomerates in Norway Lake had no flat pebbles visible (Fig. 7E). The observed beds do not match current definitions of flat-pebble conglomerates (Sepkoski, 1982; Myrow et al., 2004; Smith et al., 2020), where beds flat pebbles are the dominant clast. Instead, the beds in Norway Lake and Gene Pond more closely resemble slump conglomerates with poor sorting, variable roundness, and poor-to-moderate grading (Markello & Read, 1981; Gawthorpe, 1986; Chakraborty, 2011). Such facies are typically found near the margins of carbonate platforms, either triggered by slope instablility or tectonic activity (McIlreath & James, 1978; Cook & Mullins, 1983).

This study does not refute the potential presence of flat-pebble conglomerates elsewhere in the Randville Dolomite, though none were observed in the outcrops measured. For Randville conglomerates without evidence of desiccation, Greenman (1951) proposed formation in offshore zones as thin, brittle layers of hardened seafloor are disturbed and transported short distances. This mode of formation has since been proposed as the primary mode of flat-pebble formation (Sepkoski 1982; Myrow et al., 2004; Smith et al., 2020). Offshore conglomerates are far more frequent in Precambrian environments than modern ones, mostly disappearing by the mid-Ordovician (Sepkoski, 1982; Tarhan, 2018). Several non-exclusive hypotheses have been proposed to explain early cementation of offshore sediment, including a lack of metazoan bioturbation (Sepkoski et al., 1991; Pruss et al., 2010), generally elevated carbonate saturation in Precambrian seas (Pruss et al., 2010), or redox conditions favoring carbonate precipitation via sulfate reduction (Sepkoski, 1982; Sepkoski et al., 1991; Myrow et al., 2004). Greenman noted elevated concentrations of authigenic pyrite in Randville conglomerates and interpreted them as evidence of sulfate reduction.

5.1.2. Oolites

Oolites have been reported in certain Randville deposits that were not visited by this study (Clements & Smyth, 1899; Greenman, 1951; Gair & Weir, 1956), and none were observed in Lake Antoine, Norway Lake, Strawberry Lake, or Bacco Quarry. Ooids are mostly reported in the Amasa Uplift region northwest of Iron Mountain, near Michigamme Mountain and Fence River (Clements & Smyth, 1899; Greenman, 1951; Gair & Weir, 1956). The only other reported location is from the town of Norway near Iron Mountain (not to be confused with Norway Lake), less than one kilometer east of Strawberry Lake (Greenman, 1951). Randville ooids are 1–2 mm in diameter and circular to oval in shape, with some examples of compound nuclei. Nuclei differ between regions: Amasa ooids in the north have quartz nuclei, while Norway ooids have carbonate nuclei. Dolomitization has removed many details, but original fabrics surrounding nuclei appear to have been radial (Greenman, 1951). Local stratigraphic context for Randville oolites remains lacking, with few descriptions of bedding thickness or contacts. The Norway oolite is described from two isolated outcrops 400 m apart, interpreted as representing a single unit 10 m thick, but this data has not been corroborated (Greenman, 1951).

Several hypotheses exist regarding carbonate ooid formation, with differences mostly focusing on relative biogenicity (Davies et al., 1978; Simone, 1980; Duguid et al., 2010; Diaz & Eberli, 2019). One uniting principle is that ooids require high-energy, agitated waters to grow, with periodic intervals of rest. Modern environments include beaches, sandbars, and shoals influenced by waves and tides. In contrast, many previously discussed sedimentary features of the Randville Dolomite (planar dolomite, infrequent scours and conglomerates) broadly indicate less agitated environments. In the absence of detailed oolite stratigraphy, this study interprets Randville oolites as shallower shoal deposits on the edges of calmer environments, such as the outer shelf of a

carbonate platform.

Overall, the majority of Randville sedimentary structures support a relatively calm, unrestricted depositional environment punctuated by minor disturbances. Instead of frequent tidal activity, planar dolomites are occasionally disrupted by scours, most likely from storm activity. The presence of poorly-sorted conglomerates and slumping also supports a calm environment periodically agitated by slope failure or tectonic activity. The combination of facies are interpreted as the outer margins of a carbonate platform, with stromatolites on interior lagoons, slumping near slopes, and ooids forming shoals. Such environments occur near the edges of the modern Bahamas (Hine and Neumann, 1977; Schlager and Ginsburg, 1981; Bergman et al., 2010). The possibility for other environments remains possible, especially given the limited extent of known exposure. The potential presence of mud cracks would indicate periods of subaerial exposure and supratidal conditions. Further investigation of oolites could determine if Randville ooids formed locally on shoals or were transported to deeper margin environments after formation.

5.2. Microbial deposits

Stromatolites have been described in every region of Randville exposure except the Amasa Uplift and the Felch region, the latter due to higher degrees of metamorphism (Dryden, 1962). Many stromatolites appear as individual structures rather than laterally extensive beds (Fig. 4A, 5A, C, 6C), either completely isolated or separated from neighboring structures by several dm. The presence of stromatolites does not mean an absence of any disturbance, as exhibited by a conglomerate deposit overlying NL stromatolites. In most localities, facies gradually transition from relatively scoured dolomite to more laminated beds, culminating in stromatolite deposits (Fig. 3). The average cycle is around two meters tall, before beginning a new cycle with a scoured dolomite layer.

5.2.1. Inclined stromatolites

Most stromatolites grow vertically or perpendicular to their substrate. Inclined stromatolites, with subsequent laminae displaced from surface-normal in a consistent or shifting direction, are less frequent but occur throughout Earth history (Nordeng, 1963; Hoffman, 1967; Horodyski, 1983; Awramik & Vanyo, 1986; Kusky & Vanyo, 1991; Petryshyn & Corsetti, 2011; Tosti & Riding, 2017a). The number and diversity of inclined stromatolite morphology in the Randville Dolomite differs from other Paleoproterozoic carbonates in the region such as the Kona Dolomite (Nordeng, 1963). Inclined stromatolites are only observed in the Iron Mountain area (Fig. 6), both in our study (LA1, LA2, SL2) and in previous research which only described Lake Antoine (LA1) (Richardson, 1949; Greenman, 1951; Nordeng, 1963).

The inclined nature of Randville stromatolites has four potential explanations: (1) metamorphic stress on stromatolites, (2) phototropic stromatolite growth, (3) flow-oriented stromatolite growth, or (4) soft-sediment deformation. Metamorphic stress and phototropic growth were proposed by previous Randville studies (Richardson, 1949; Nordeng, 1963), while this study adds discussion of flow-oriented growth and soft-sediment deformation.

The earliest description assumed post-depositional shearing had altered stromatolite shapes (Richardson, 1949). While the stromatolites have certainly been altered to greenschist facies (James, 1955; Bayley et al., 1966), several lines of evidence argue against shearing as the influence of inclination. Outcrops such as LA2 have vertically-oriented nodular stromatolites and steeply-inclined columns in the same unit, dm away from each other (Figs. 5A and 6C). Furthermore, the lamination in LA2′s inclined column is laterally linked smoothly with laterally-adjacent planar layers (Fig. 6C). The lack of noticeable shear in nearby stromatolites or in adjacent layers supports the inclined LA2 column as a primary feature. In LA1, inclined stromatolites gradually shift their angle of growth from ~60 degrees from vertical to fully vertical over 30 cm, situated between two planar-laminated beds (Fig. 6A, B). Such shifts are more likely ascribed to changes in depositional condition than micro-scale shifts in metamorphic shear. SL2 stromatolites also have low inheritance between layers, shifting between different angles of growth over several centimeters (Fig. 6D, E). Finally, shearing is not observed in petrographic thin sections from any stromatolite locality.

Nordeng (1963) proposed that LA1 stromatolites were inclined due to phototropic growth.

Living stromatolites contain thousands of taxa performing many different metabolisms such as oxygenic and anoxygenic photosynthesis, aerobic and anaerobic respiration, etc. Stromatolite growth involves complex interactions between these microbial metabolisms and their depositional environment, but broad patterns have been observed between biology and morphology. Photosynthesizing microbes typically comprise the uppermost layers of microbial mats, with oxygenic photosynthesis and other forms of phototrophy fostering carbonate precipitation. The cyclical progression between photosynthesis, carbonate growth, and subsequent microbial migration upward toward light or nutrient sources remains a fundamental paradigm of stromatolite formation (Chafetz & Buczynski, 1992, Merz-Preiss & Riding, 1999, Riding, 2000; Arp et al., 2001; Stal, 2012). In some cases, living stromatolites not only exhibit phototropic activity upwards, but also towards the equator in the direction of more sunlight (Awramik & Vanyo, 1986; Kusky & Vanyo, 1991), especially in low-energy environments. Nordeng (1963) used the angle of Randville (LA1) and Kona stromatolites to estimate a paleolatitude around 30 degrees N, though his stromatolite growth angle (22 degrees from vertical) underestimates the ~60-degree angle of many other samples. Furthermore, the orientation of stromatolite growth is in opposing directions in different locations along NW-SE strike: columns in LA1 and LA2 grow upward to the east, while columns in SL2 grow upward to the west. However, direct correlation of strikes and dips is difficult with such isolated, distant exposures in a structurally complex area.

Inclined stromatolites can also be formed by the influence of flowing water, also proposed by Richardson (1949) for LA1 columns. Evidence for current-angled stromatolites typically comes from higher-energy peritidal environments, with stromatolite growth upwards into current flow (Hoffman, 1967; Horodyski, 1983; Tosti & Riding, 2017a). This counter-current growth occurs as particulate matter accretes to the leading edge of adhesive microbial mats (Tosti & Riding, 2017a). As previously discussed, the majority of Randville sedimentary structures indicate a relatively calm platform environment punctuated by storms or large waves. However, examining the morphology of LA1 stromatolites supports the influence of water flow over phototropism. First, stromatolites immediately overlie an erosional surface cutting into planar-laminated dolomite, indicating a shift from calm to energetic waters (Fig. 6A). Subsequent stromatolite initiation and growth occurred on slower timescales after the erosive event, indicating longer time-scales of sedimentation. As stromatolites grow upward, growth angles grow increasingly vertical and eventually grade back into planar dolomite, as expected if water movement diminished over time. Finally, LA1 stromatolite margins are relatively ragged, with individual layers expanding and contracting compared with previous generations (Fig. 6B). Similar margins are observed when stromatolites grow in environments with varying rates of sedimentation (Barlow et al., 2016; Tosti & Riding, 2017b).

Other inclined structures are not as easily explained by current action. For example, LA2 is 400 m from LA1, but the single inclined stromatolite observed has a consistent angle of growth and is laterally-linked with surrounding planar dolomites (Fig. 6C). One potential explanation for such inclined structures is soft-sediment deformation such as slumping (Mills, 1983; van Loon, 2009). The dominance of planar-laminated dolomite with less ambiguous stromatolites in Randville exposures supports a low-energy carbonate platform. In such environments, slumping can occur on the outer margins due to slope instability (Schlager & Chermak, 1979; Betzler et al., 1999), or by

tectonic activity during deposition (Spalluto et al., 2007; Mastrogiacomo et al., 2012). While some isolated Randville structures potentially represent soft-sediment deformation (Fig. 6C), the ragged margins between inclined columns in LA1 (Fig. 6B) more closely resemble individual stromatolites. Further study of Randville stromatolites is required to distinguish different forms of inclination, but evidence currently suggests at least some forms represent stromatolites.

5.2.2. Dendrolite-like structures

Dendrolites are microbialites defined by non-laminated, dendritic (branching) fabrics (Riding, 1991), as opposed to laminated stromatolites. The internal structure of dendrolites is usually composed of branching microfossils such as *Epiphyton* and *Renalcis* (Pratt, 1984; Riding, 1991), though modern examples can be made from single-filament microbes (Bradley et al., 2017; Suosaari et al., 2018). Microfossils inside dendrolites have a diverse range of forms, but are typically (1) composed of micrite, (2) oriented and elongated vertically, (3) have branching morphologies. Individual microfossils range from sub-mm to 1 cm high, typically between 1 and 2 mm high. Clusters of branching microfossils form macroscopic dendrolites, either as individual "shrubs" or as larger domes and columns.

The micritic, occasionally branching microstructures in Norway Lake laminated dolomite (Fig. 8D, E) most closely resemble dendrolitic microfossils but are unique in several ways. Unlike most dendrolites, where microfossils build upward on each other into shrubs or domes, the Norway Lake microstructures are confined to individual planar laminations. Most microstructures are unbranched or branch only once (Fig. 8D, C), whereas *Epiphyton, Renalcis,* and similar microfossils branch frequently (Pratt, 1984; Riding, 1991). Finally, if the micritic Norway Lake features formed in a similar fashion to dendrolites, they would be far older than other examples. Dendrolites are most abundant from the Neoproterozoic to the Ordovician (Pratt, 1984; Riding, 1991; Rowland & Shapiro, 2002; Fraiser & Corsetti, 2003; Shapiro & Rigby, 2004) and are relatively rare in modern environments (Bradley et al., 2017; Suosaari et al., 2018). As far as we are aware, the Norway Lake microstructures are the first features resembling dendrolites described before the Neoproterozoic. The structures were only observed in one thin section ~0.7 m from the base of the Norway Lake section (Fig. 2), forming 5 layers within 2 cm of laminated dolomite. Further investigation of collected samples, the Norway Lake area, and other Randville deposits will provide further detail on the sedimentary and biological relevance of these unique microbial structures, potentially the earliest described dendrolites.

5.3. Isotope geochemistry

Measured values of $\delta^{13}C$ (0.51 to 1.68 ‰) and $\delta^{18}O$ (−8.11 to −5.91 ‰) in Fig. 10 and Table 1 match previous Randville measurements by Bekker et al., 2006 from Norway Lake and Iron Mountain ($\delta^{13}C$: −0.4 to 1.5 ‰; $\delta^{18}O$: −12.0 to −5.6 ‰). Such values also align with the average $\delta^{13}C$ in most marine carbonates throughout Earth history (Shields & Veizer, 2002). However, the Randville Dolomite differs from many carbonates deposited around the Lomagundi-Jatuli Excursion (LJE) 2.3–2.0 Ga, with $\delta^{13}C$ above + 5 ‰ (Prave et al., 2022; Hodgskiss et al., 2023), including the Kona Dolomite ~75 km to the northeast. Randville and Kona deposits are correlated within the Chocolay Group, but Kona $\delta^{13}C$ values are usually above 5 ‰ and as high as 10 ‰ (Bekker et al., 2006). While the chemical data from this study is from a relatively limited sample set, the isotopic and elemental values measured align well with previous isotopic studies on nearby exposures and ones in other Randville outcrops (Bekker et al., 2006). Further Randville investigation may reveal a wider spread of isotopic data, but for now, data from multiple surveys and locations place $\delta^{13}C$ in the formation between 0 and 3 ‰, lower than many other LJE carbonates. Several explanations have been proposed for isotopic differences between the Kona and Randville Dolomite: (1) post-depositional alteration, (2) asynchronous timing, and (3) environmental differences.

5.3.1. Alteration

The Randville and Kona Dolomite have experienced regional greenschist facies metamorphism at minimum (James, 1955; Bayley et al., 1966). Kona deposits entirely lie within the least metamorphosed "chlorite zone" of James, 1955, interpreted as lower greenschist-facies. The same study reported a wider variety of metamorphic facies in Randville deposits. Norway Lake samples (NL) come from a "chlorite zone" similar to the Kona Dolomite, also interpreted as lower greenschist facies (James, 1955). Iron Mountain samples (LA1, LA2, SL2) represent a slightly more metamorphosed "biotite zone" in neighboring silicate rocks, interpreted as upper greenschist facies (James, 1955). Despite slightly differing grades of regional metamorphism, the petrography of each Randville location in this study includes well-preserved micritic textures such as dendrolites, rip-up clasts, and sub-mm stromatolite layers. Compared with previous Kona Dolomite petrography, Randville samples from this study had more well-preserved petrographic textures including higher amounts of micrite, less recrystallized spar, and lower amounts of metamorphic tremolite (Gair & Thaden, 1968; Wohlabaugh & Mancuso, 1990; Giannecchini et al., 2023).

While the petrography and regional metamorphism of the Randville Dolomite resembles other LJE deposits where $\delta^{13}C$ is interpreted as a signature of seawater DIC (Hodgskiss et al., 2023), several proxies were examined to assess local alteration patterns. Meteoric alteration can influence $\delta^{13}C$ in ancient carbonates, though to a lesser extent than other chemical signatures such as $\delta^{18}O$, Mn, and Sr (Lohmann, 1988; Allan & Matthews, 1990; Kaufman & Knoll, 1995). In the Randville Dolomite, consistently depleted $\delta^{18}O$ values around −7‰ are likely due to re-equilibration during meteoric water–rock interactions (Fig. 10A, Table 1), but the lack of correlation between $\delta^{13}C$ and $\delta^{18}O$ indicates that oxygen was more susceptible to alteration, a trend commonly observed in Precambrian carbonates (Kaufman & Knoll, 1995). In contrast, depleted $\delta^{13}C$ often occurs in replacement cements in vadose and phreatic alteration zones (Lohmann et al., 1988). A relative lack of sparry cements in Randville samples, especially in areas drilled for geochemistry data, indicates that such alteration did not have a major impact on $\delta^{13}C$ (Figs. 8 and 9).

Mn/Sr ratios were also calculated to compare with previous measurements in Randville samples (Fig. 10B, Table 1). High levels of Mn paired with low levels of Sr have been interpreted as alteration from the infiltration of rainwater after burial, with low ratios potentially indicating less meteoric alteration (Veizer, 1983; Kaufman et al., 1993; Kaufman & Knoll, 1995). Samples from Norway Lake and Lake Antoine had low Mn/Sr ratios (1–5), while Strawberry Lake values were significantly higher (18–31). Kaufman & Knoll, 1995 suggested an upper Mn/Sr threshold of 10 for investigating $\delta^{13}C$ in Neoproterozoic carbonates, but also noted the threshold was subject to interpretation, since major isotopes are less sensitive to meteoric influence than Sr. For example, Bekker et al., 2006 considered some Kona Dolomite samples with Mn/Sr values up to 120 as valid for investigating $\delta^{13}C$, while other samples with similar values were discounted. Broad trends in the study's discounted samples include enriched Mn and depleted $\delta^{18}O$ and Sr, but the exact numerical thresholds for inclusion were not discussed. In short, Kaufman & Knoll, 1995 noted that synthesizing petrographic, elemental, and isotopic data provides useful screens for altered $\delta^{13}C$, but data selection still requires case-by-case analysis.

For example, Strawberry Lake samples had the highest Mn/Sr ratios (18–31) recorded in this study (Fig. 10B) and compared with previous Randville maximum values (23) from Bekker et al., 2006. The Mn/Sr measure of alteration broadly matches increasing metamorphic grades previously observed in Iron Mountain (James, 1955). However, the petrography of Strawberry Lake samples is no more recrystallized than Lake Antoine or Norway Lake deposits (Figs. 8 and 9). Critically, $\delta^{13}C$ values in Strawberry Lake are intermediary between the other locations with lower Mn/Sr ratios (Fig. 10B), instead of forming an isotopic

outlier. Therefore, while Strawberry Lake samples have different patterns of meteoric alteration than Norway Lake or Lake Antoine, their isotopic similarity increases confidence in an original seawater signature. With similar metamorphic grades and alteration indices, $\delta^{13}C$ patterns between the Randville and Kona Dolomite are unlikely to stem from meteoric, metamorphic, or other post-depositional effects.

5.3.2. Correlation with the Kona Dolomite

The timing of Randville and Kona deposits during the LJE could potentially explain their isotopic differences (Fig. 2). Ages compiled from Paleoproterozoic carbonates give a maximum acceptable LJE window between 2318 to 2057 Ma, and a minimum window between 2221 and 2106 Ga (Martin et al., 2013; Rasmussen et al., 2024). Many carbonates deposited immediately before or after these windows have $\delta^{13}C \sim 0$ ‰, while many within the LJE are at least 5 ‰ (Martin et al., 2013; Hodgskiss et al., 2023). Elevated $\delta^{13}C$ in the Kona (5–10 ‰) fit into the LJE's maximum and minimum windows (2174 Ma, Rasmussen et al., 2024), while the Randville Dolomite's age remains poorly defined between 2306 ± 9 Ma and 2115 ± 5 Ma (Vallini et al., 2006, see Geological Setting). Though the Randville and Kona Dolomite are frequently correlated based on Chocolay Group stratigraphy, current age estimates could place Randville deposition before, during, or after Kona carbonates.

The lack of defined dates for Randville deposits leads to several scenarios explaining depleted $\delta^{13}C$. In chronological order: (1) early LJE deposition (2.3–2.2 Ga) before global signatures reached their peak, (2) peak LJE deposition in a different environment than the Kona Dolomite (2.2–2.1 Ga), or (3) deposition after the LJE (post-2.1 Ga). The Randville's true minimum constraint is 1874 ± 9 Ma (Schneider et al., 2002), but this overlying date is separated by a major unconformity. Metamorphic xenotime ages from conformably underlying Sturgeon Quartzite (2115 ± 5 Ma) are likely closer to the Randville's true age (Vallini et al., 2006). For example, xenotime beneath the Kona Dolomite produced a minimum age at 2131 ± 13 Ma (Vallini et al., 2006), closely matching immediately overlying zircon dates of 2174 ± 9 Ma (Rasmussen et al., 2024). Similar error ranges for Sturgeon xenotime ages would either place the Randville in the peak LJE (2.2–2.1 Ga), or in the later stages (2.1–2.0 Ga). In summary, despite wide age constraints, the Randville Dolomite was deposited within the broadest LJE window (2.3–2.0 Ga) and very likely around the narrowest definition (2.2–2.1 Ga) when many other carbonates had elevated $\delta^{13}C$ values.

5.3.3. Facies dependence

If alteration or timing cannot explain patterns in Randville and Kona $\delta^{13}C$, differences in Paleoproterozoic environments provide the most likely explanation. The two carbonates were deposited in shallow marine waters but represent distinct environments. Randville deposits are defined by planar laminated dolomite intermittently interrupted by scours, slumps and conglomerates (Fig. 7). Petrography also supports alternating periods of low energy (planar beds with dendrolitic microstructures) with periodic disruption (small rip-up clasts) (Figs. 8 and 9). Evidence for restriction or subaerial exposure are either rare (mud cracks) or not observed (evaporite pseudomorphs). The Randville depositional environment represents a calm margin of a carbonate platform, influenced by marine waters with unrestricted, open-marine isotope signatures.

The Kona Dolomite has larger exposures and a more well-defined stratigraphy. Facies shift over time and distance but are broadly defined by shallower supratidal environments to the west and deeper subtidal zones to the east (Gair & Thaden, 1968; Taylor, 1972; Larue, 1981; Wohlabaugh & Mancuso, 1990; Giannecchini et al., 2023). Unlike the Randville Dolomite, western Kona deposits frequently show evidence for supratidal conditions, including mud cracks and pseudomorphs of gypsum crystals and rosettes. Associated stromatolites form abundant, low-relief beds (<2 cm), commonly observed in modern supratidal and shallow intertidal zones (Taylor, 1972; Wohlabaugh & Mancuso, 1990). Adjacent roll-over structures form when cohesive, unlithified microbial mats are disturbed by wave or storm activity. Ooids are more abundant in Kona than Randville deposits, indicating high-energy shoals (Taylor, 1972; Wohlabaugh & Mancuso, 1990). In the eastern Kona, large stromatolite domes with at least 30 cm of seafloor relief form beds over 10 m thick in calmer, relatively deeperl waters (Twenhofel, 1919; Taylor, 1972; Wohlabaugh & Mancuso, 1990). The broader Kona environment is interpreted as a restricted lagoon, periodically separated from open marine waters by an outer barrier before flooding into overlying slates (Taylor, 1972).

Similar patterns of $\delta^{13}C$-enriched carbonates in shallower, restricted, or evaporitic basins (Kona Dolomite) vs. values ~0 ‰ in offshore, shelf, or open marine zones (Randville Dolomite) have been observed in several LJE deposits (Schidlowski et al., 1976; Melezhik et al.,1999; Frauenstein et al., 2009; Mayika et al., 2020; Prave et al., 2022). Recently, Prave et al., 2022 surveyed $\delta^{13}C$ isotopes in over 14,000 carbonates (with over 2,000 LJE carbonates) grouped into (1) intertidal-coastal sabkha, (2) nearshore-inner shelf, and (3) open-deeper marine zones. Compared with $\delta^{13}C$ before and after the LJE, intertidal-sabkha carbonates were elevated by 8.1 ± 3.8 ‰, nearshore-inner shelf carbonates by 6.2 ± 2.0 ‰, and open-deeper marine carbonates by only 1.5 ± 2.5 ‰.

While Prave et al. (2022) did not provide the depositional environment for each locality surveyed, more detailed classifications are given in Hodgskiss et al. (2023), focusing on over 9000 samples between 2.8 and 1.7 Ga. Listing environmental descriptions from each surveyed paper, the 2023 survey clarifies Prave's depositional zones into (1) sabkha-peritidal, (2) platform and mid-upper ramp, and (3) lower ramp, slope, and deep basin. While accumulated datasets from zone have C isotope peaks at 0 and 7 ‰, values over 5 ‰ are distinctly less in platform and slope zones than peritidal zones. Hodgskiss et al. (2023) classified the Randville Dolomite as sabkha-peritidal, referencing Bekker et al. (2006). Our study supports a "platform and mid-upper ramp" by Hodgskiss et al. (2023), similar to portions of the 2.2–2.3 Ga Kazput and Kungarra Formations of Western Australia (Martindale et al., 2015).

Facies-driven $\delta^{13}C$ variations are observed in many LJE carbonates, but the specific mechanisms driving these changes remain debated. In modern carbonates, shallow marine settings and restricted lakes can be enriched up to 5–6 ‰ (Aharon et al., 1977; Schidlowski et al., 1985; Swart, 2008; Swart et al., 2009; Geyman & Maloof 2019). In each case, $\delta^{13}C$ increases are driven by enhanced primary productivity in photosynthetic microbial communities, removing ^{12}C from DIC into organic matter. In certain isolated lakes and lagoons, enhanced photosynthesis and methanogenesis can even produce carbonates up to 16 ‰ (Birgel et al., 2015; Cadeau et al., 2020). In such restricted environments, methanogens fractionate and liberate ^{12}C from organic matter into methane, further concentrating local DIC with ^{13}C. Sumner (2024) uses a similar model for the global LJE: cyanobacteria expanded in shallow environments, creating local reservoirs of isotopically-light organic carbon. Methanogen activity would be boosted by this organic matter, fueling increased production of methane, which was lost to the atmosphere and removed from local DIC reservoirs (Sumner, 2024). Methane loss would be most efficient in low-solubility environments such as warm, extremely shallow, evaporative waters, which can also be areas of vigorous primary productivity as seen in modern mats (Birgel et al., 2015; Cadeau et al., 2020). In this model, the LJE ended with the expansion of various respiration metabolisms with less isotope fractionation (aerobic, sulfate reduction, nitrate reduction, etc.). For the Randville Dolomite, $\delta^{13}C$ closer to 0 could represent an environment with less methane release, either due to relative water depth or less methanogen activity (Sumner, 2024).

The removal of ^{12}C via CO_2 evaporation is another potential aspect driving elevated $\delta^{13}C$. Brine evaporation experiments have produced solutions with $\delta^{13}C$ over 10 ‰ and occasionally over 30 ‰ (Stiller et al., 1985; Horton et al., 2016), though such high values are rarely reported in modern natural environments. While some $\delta^{13}C$-enriched localities do

not contain evidence for restriction (Bekker and Eriksson, 2003), the presence of evaporites and pseudomorphs (gypsum and halite) in many LJE carbonates strongly suggests that evaporative environments played some role in localized isotope enrichment (Melezhik et al., 1999; Prave et al., 2022). Of the eight LJE-era carbonates in the Lake Superior region, the only two units with reported evaporites (Kona, Gordon Lake) are also the only units with $\delta^{13}C$ over 5 ‰ (Taylor 1972; Cameron 1983; Chandler 1988; Wohlabaugh & Mancuso 1990; Bekker et al., 2006). Further investigations could still find restricted facies in the other six units (Bad River, Denham, Glen Township, Randville, Saunders, Trout Lake), but our inferred unrestricted platform environment for the Randville lowers the likelihood in this case.

The Randville Dolomite was deposited near the margins of a relatively calm carbonate platform ~2.2 Ga. Observed scouring is infrequent, influenced by periodic events instead of nearshore waves or tides. Clastic influence from shorelines was variable, but often minimal. Microbial communities covered benthic substrates during calmer intervals, forming domes and cones. Occasional disturbances influenced the morphology of microbial colonies, forming inclined columns and occasionally ripping up mat pieces. While limited exposure prevents further examination of lateral or temporal changes in Randville environments, our results reveal a distinctly different environment from the restricted, evaporitic coast of the neighboring Kona Dolomite. Our research indicates that isotopic differences between the $\delta^{13}C$-"depleted" Randville and the enriched Kona are best explained by these environmental differences.

6. Conclusion

The LJE is defined by carbonates with extremely enriched $\delta^{13}C$ above 5 ‰, but not all locations during this interval contain such extreme isotopic signatures. Differences between the Randville Dolomite (0–3 ‰) and Kona Dolomite (+5 to 10 ‰) are best explained by differences in depositional environments. Throughout the Randville Dolomite, most sedimentary evidence indicates a relatively calm carbonate platform with infrequent scours and no evaporite pseudomorphs. In comparison, previous evidence from the Kona Dolomite supports deposition in a restricted, evaporitic marine basin. Elevated $\delta^{13}C$ in Kona deposits is likely due to enhanced loss of ^{12}C from evaporitic degassing and enhanced carbon fixation in extensive, shallow microbial mats. While diverse microbial facies are present in the Randville Dolomite, they are less laterally-extensive or temporally-persistent as Kona stromatolites. Similar facies-dependent patterns (heavier evaporitic, lighter open-marinel) are observed in other LJE carbonates in the Lake Superior region and globally. While facies dependence cannot explain all aspects of the LJE, our data support the idea that local $\delta^{13}C$ effects can explain at least some LJE excursions.

CRediT authorship contribution statement

Garrett D. Brown: Writing – original draft, Investigation, Funding acquisition, Formal analysis, Data curation, Conceptualization. **Maya L. Giannecchini:** Writing – review & editing, Investigation, Funding acquisition, Formal analysis, Data curation. **Cory M. Redman:** Writing – review & editing, Validation, Investigation, Data curation. **Ian Z. Winkelstern:** Writing – review & editing, Validation. **Dylan T. Wilmeth:** Writing – review & editing, Supervision, Methodology, Investigation, Data curation, Conceptualization.

Declaration of competing interest

The authors declare that they have no known competing financial interests or personal relationships that could have appeared to influence the work reported in this paper.

Acknowledgements

This work was supported by a Modified Student Summer Scholar Grant and a Kindschi Fellowship from Grand Valley State University to G.D. Brown. We thank Ginny Peterson at GVSU for access to petrographic software, Kyger Lohmann at the University of Michigan for isotopic analyses, and Stephanie Bilinovich at GVSU for ICP-OES access. We also thank the private citizens of Iron Mountain and Norway, MI for access to Randville exposures.

Data availability

Data will be made available on request.

References

Aharon, P., Kolodny, Y., Sass, E., 1977. Recent hot brine dolomitization in the" solar lake," gulf of elat, isotopici, chemical, and mineralogical study. J. Geol. 85, 27–48.
Allan, J.R., Matthews, R.K., 1990. Isotope signatures associated with early meteoric diagenesis. In: Tucker, M.E., Bathurst, R.G.C. (Eds.), Carbonate Diagenesis. Wiley, pp. 197–217. https://doi.org/10.1002/9781444304510.ch16.
Arp, G., 2001. Photosynthesis-induced biofilm calcification and calcium concentrations in Phanerozoic Oceans. Science 292, 1701–1704. https://doi.org/10.1126/science.1057204.
Awramik, S.M., Vanyo, J.P., 1986. Heliotropism in modern stromatolites. Science 231, 1279–1281.
Barlow, E., Van Kranendonk, M.J., Yamaguchi, K.E., Ikehara, M., Lepland, A., 2016. Lithostratigraphic analysis of a new stromatolite–thrombolite reef from across the rise of atmospheric oxygen in the Paleoproterozoic Turee Creek Group, Western Australia. Geobiology 14, 317–343. https://doi.org/10.1111/gbi.12175.
Bayley, R.W., 1959. Geology of the Lake Mary Quadrangle, Iron County, Michigan. USGS Bull. 1077. https://doi.org/10.3133/b1077.
Bayley, R.W., Dutton, C.E., Lamey, C.A., 1966. Geology of the Menominee iron-bearing district, Dickinson County, Michigan, and Florence and Marinette Counties, Wisconsin, Professional Paper. U.S. Geol. Surv. Prof. Paper 513. https://doi.org/10.3133/pp513.
Bekker, A., Eriksson, K.A., 2003. A Paleoproterozoic drowned carbonate platform on the southeastern margin of the Wyoming Craton: a record of the Kenorland breakup. Precambrian Research 120, 327–364. https://doi.org/10.1016/S0301-9268(02)00165-1.
Bekker, A., Holland, H.D., 2012. Oxygen overshoot and recovery during the early Paleoproterozoic. Earth Planet. Sci. Lett. 317–318, 295–304. https://doi.org/10.1016/j.epsl.2011.12.012.
Bekker, A., Karhu, J.A., Kaufman, A.J., 2006. Carbon isotope record for the onset of the Lomagundi carbon isotope excursion in the Great Lakes area, North America. Precambr. Res. 148, 145–180. https://doi.org/10.1016/j.precamres.2006.03.008.
Bergman, K.L., Westphal, H., Janson, X., Poiriez, A., Eberli, G.P., 2010. Controlling Parameters on Facies Geometries of the Bahamas, an Isolated Carbonate Platform Environment. In: Westphal, H., Riegl, B., Eberli, G.P. (Eds.), Carbonate Depositional Systems: Assessing Dimensions and Controlling Parameters. Springer Netherlands, Dordrecht, pp. 5–80. https://doi.org/10.1007/978-90-481-9364-6_2.
Betzler, C., Reijmer, J.J.G., Bernet, K., Eberli, G.P., Anselmetti, F.S., 1999. Sedimentary patterns and geometries of the Bahamian outer carbonate ramp (Miocene–Lower Pliocene, Great Bahama Bank). Sedimentology 46, 1127–1143. https://doi.org/10.1046/j.1365-3091.1999.00268.x.
Birgel, D., Meister, P., Lundberg, R., Horath, T.D., Bontognali, T.R.R., Bahniuk, A.M., de Rezende, C.E., Vasconcelos, C., McKenzie, J.A., 2015. Methanogenesis produces strong 13 C enrichment in stromatolites of Lagoa Salgada, Brazil: a modern analogue for Palaeo-/Neoproterozoic stromatolites? Geobiology 13, 245–266. https://doi.org/10.1111/gbi.12130.
Bradley, J.A., Daille, L.K., Trivedi, C.B., Bojanowski, C.L., Stamps, B.W., Stevenson, B.S., Nunn, H.S., Johnson, H.A., Loyd, S.J., Berelson, W.M., Corsetti, F.A., Spear, J.R., 2017. Carbonate-rich dendrolitic cones: insights into a modern analog for incipient microbialite formation, Little Hot Creek, Long Valley Caldera, California. NPJ Biofilms Microbiom. 3, 32. https://doi.org/10.1038/s41522-017-0041-2.
Buchan, K.L., Halls, H.C., Mortensen, J.K., 1996. Paleomagnetism, U–Pb geochronology, and geochemistry of Marathon dykes, Superior Province, and comparison with the Fort Frances swarm. Can. J. Earth Sci. 33, 1583–1595. https://doi.org/10.1139/e96-120.
Cadeau, P., Jézéquel, D., Leboulanger, C., Fouilland, E., LeFloc'h, E., Chaduteau, C., Milesi, V., Guélard, J., Sarazin, G., Katz, A., d'Amore, S., Bernard, C., Ader, M., 2020. Carbon isotope evidence for large methane emissions to the Proterozoic atmosphere. Sci Rep 10, 18186. https://doi.org/10.1038/s41598-020-75100-x.
Cameron, E.M., 1983. Evidence from early Proterozoic anhydrite for sulphur isotopic partitioning in Precambrian oceans. Nature 304, 54–56. https://doi.org/10.1038/304054a0.
Cannon, W.F., Gair, J.E., 1970. A revision of stratigraphic nomenclature of middle Precambrian rocks in northern Michigan. Geol. Soc. Am Bull. 81.
Chafetz, H.S., Buczynski, C., 1992. Bacterially induced lithification of microbial mats. PALAIOS 7, 277. https://doi.org/10.2307/3514973.

Chakraborty, P.P., 2011. Slides, soft-sediment deformations, and mass flows from Proterozoic Lakheri Limestone Formation, Vindhyan Supergroup, central India, and their implications towards basin tectonics. Facies 57, 331–349. https://doi.org/10.1007/s10347-010-0241-1.
Chandler, F.W., 1988. Diagenesis of sabkha-related, sulphate nodules in the early Proterozoic Gordon Lake formation, Ontario, Canada. Carbonates Evaporites 3, 75–94. https://doi.org/10.1007/BF03174414.
Clements, J.M., Smyth, H.L., 1899. The Crystal Falls iron-bearing district of Michigan. U. S. Geol. Surv. 19th Ann. Rept.
Cook, H.E., Mullins, H.T., 1983. Basin Margin Environment. In: Carbonate Depositional Environments. American Association of Petroleum Geologists. https://doi.org/10.1306/M33429C18.
Davies, P.J., Bubela, B., Ferguson, J., 1978. The formation of ooids. Sedimentology 25, 703–730.
Diaz, M.R., Eberli, G.P., 2019. Decoding the mechanism of formation in marine ooids: a review. Earth Sci. Rev. 190, 536–556.
Dryden, D.A., 1962. Petrology and petrofabrics of the Randville Dolomite in the Felch Mountain Trough, Dickinson County, Michigan. (Ph.D. Thesis). Michigan State Institute, Lansing.
Duguid, S.M., Kyser, T.K., James, N.P., Rankey, E.C., 2010. Microbes and ooids. J. Sediment. Res. 80, 236–251.
Fraiser, M.L., Corsetti, F.A., 2003. Neoproterozoic carbonate shrubs: interplay of microbial activity and unusual environmental conditions in post-Snowball Earth oceans. PALAIOS 18, 378–387.
Frauenstein, F., Veizer, J., Beukes, N., Van Niekerk, H.S., Coetzee, L.L., 2009. Transvaal Supergroup carbonates: Implications for Paleoproterozoic δ18O and δ13C records. Precambr. Res. 175, 149–160. https://doi.org/10.1016/j.precamres.2009.09.005.
Gair, J.E., 1975. Bedrock geology and ore deposits of the Palmer Quadrangle, Marquette County, Michigan. U.S. Geol. Surv. Prof. Paper 769. https://doi.org/10.3133/pp769.
Gair, J.E., Thaden, R.E., 1968. Geology of the Marquette and Sands Quadrangles Marquette County Michigan. US Geol. Surv. Prof. Paper 397. https://doi.org/10.3133/pp397.
Gair, J.E., Wier, K.L., 1956. Geology of the Kiernan Quadrangle, Iron County, Michigan. USGS Bull. 1044. https://doi.org/10.3133/b1044.
Gawthorpe, R.L., 1986. Sedimentation during carbonate ramp-to-slope evolution in a tectonically active area: Bowland Basin (Dinantian), northern England. Sedimentology 33, 185–206. https://doi.org/10.1111/j.1365-3091.1986.tb00531.x.
Geyman, E.C., Maloof, A.C., 2019. A diurnal carbon engine explains 13C-enriched carbonates without increasing the global production of oxygen. Proc. Natl. Acad. Sci. 116, 24433–24439.
Giannecchini, M., Brown, G., Redman, C., Winkelstern, I.Z. and Wilmeth, D., 2023. Stratigraphy, petrography, and carbon isotope variability among stromatolites during the 2.2 Ga Lomagundi-Jatuli Event. In: Geological Society of America Abstracts, vol. 55.
Greenman, N.N., 1951. The origin of the Randville Dolomite of Dickinson and Iron Counties, Michigan. Ph.D. Thesis. University of Chicago, Chicago.
Hawkesworth, C., Cawood, P.A., Dhuime, B., 2019. Rates of generation and growth of the continental crust. Geosci. Front. 10, 165–173. https://doi.org/10.1016/j.gsf.2018.02.004.
Hine, A.C., Neumann, A.C., 1977. Shallow Carbonate-Bank-Margin Growth and Structure, Little Bahama Bank, Bahamas1. AAPG Bulletin 61, 376–406. https://doi.org/10.1306/C1EA3CBC-16C9-11D7-8645000102C1865D.
Hodgskiss, M.S.W., Crockford, P.W., Turchyn, A.V., 2023. Deconstructing the Lomagundi-Jatuli Carbon Isotope Excursion. Annu. Rev. Earth Planet. Sci. 51, 301–330. https://doi.org/10.1146/annurev-earth-031621-071250.
Hoffman, P., 1967. Algal Stromatolites: Use in Stratigraphic Correlation and Paleocurrent Determination. Science, New Series 157, 1043–1045.
Horodyski, R.J., 1983. Sedimentary geology and stromatolites of the middle proterozoic belt supergroup, Glacier National Park, Montana. Precambr. Res. 20, 391–425.
Horton, T.W., Defliese, W.F., Tripati, A.K., Oze, C., 2016. Evaporation induced 18O and 13C enrichment in lake systems: a global perspective on hydrologic balance effects. Quat. Sci. Rev., Water Isotope Syst. 131, 365–379. https://doi.org/10.1016/j.quascirev.2015.06.030.
Jacquemyn, C., Jackson, M.D., Hampson, G.J., John, C.M., Cantrell, D.L., Zűhlke, R., AbuBshait, A., Lindsay, R.F., Monsen, R., 2018. Geometry, spatial arrangement and origin of carbonate grain-dominated, scour-fill and event-bed deposits: Late Jurassic Jubaila Formation and Arab-D Member, Saudi Arabia. Sedimentology 65, 1043–1066. https://doi.org/10.1111/sed.12414.
James, H.L., 1955. Zones of regional metamorphism in the precambrian of Northern Michigan. GSA Bull. 66, 1455–1488. https://doi.org/10.1130/0016-7606(1955)66[1455:ZORMIT]2.0.CO;2.
James, H.L., Clark, L.D., Lamey, C.A., Pettijohn, F.J., Freedman, J., Trow, J., Wier, K.L., 1961. Geology of Central Dickinson County, Michigan. U.S. Geol. Surv. Prof. Paper 310. https://doi.org/10.3133/pp310.
Karhu, J.A., Holland, H.D., 1996. Carbon isotopes and the rise of atmospheric oxygen. Geology 24, 867–870. https://doi.org/10.1130/0091-7613(1996)024<0867:CIATRO>2.3.CO;2.
Kaufman, A.J., Knoll, A.H., 1995. Neoproterozoic variations in the C-isotopic composition of seawater: stratigraphic and biogeochemical implications. Precambr. Res. 73, 27–49. https://doi.org/10.1016/0301-9268(94)00070-8.
Kaufman, A.J., Jacobsen, S.B., Knoll, A.H., 1993. The Vendian record of Sr and C isotopic variations in seawater: Implications for tectonics and paleoclimate. Earth and Planetary Science Letters 120, 409–430. https://doi.org/10.1016/0012-821X(93)90254-7.
Kusky, T.M., Vanyo, J.P., 1991. Plate reconstructions using stromatolite heliotropism: principles and applications. J. Geol. 99, 321–335.
Larue, D.K., 1981. The Chocolay Group, Lake Superior region, U.S.A.: Sedimentologic evidence for deposition in basinal and platform settings on an early Proterozoic craton. GSA Bull. 92, 417–435. https://doi.org/10.1130/0016-7606(1981)92<417:TCGLSR>2.0.CO;2.
Lohmann, K.C., 1988. Geochemical patterns of meteoric diagenetic systems and their application to studies of paleokarst. In: James, N.P., Choquette, P.W. (Eds.), Paleokarst. Springer, New York, New York, NY, pp. 58–80. https://doi.org/10.1007/978-1-4612-3748-8_3.
Markello, J.R., Read, J.F., 1981. Carbonate ramp-to-deeper shale shelf transitions of an Upper Cambrian intrashelf basin, Nolichucky Formation, Southwest Virginia Appalachians. Sedimentology 28, 573–597. https://doi.org/10.1111/j.1365-3091.1981.tb01702.x.
Martindale, R.C., Strauss, J.V., Sperling, E.A., Johnson, J.E., Van Kranendonk, M.J., Flannery, D., French, K., Lepot, K., Mazumder, R., Rice, M.S., Schrag, D.P., Summons, R., Walter, M., Abelson, J., Knoll, A.H., 2015. Sedimentology, chemostratigraphy, and stromatolites of lower Paleoproterozoic carbonates, Turee Creek Group, Western Australia. Precambr. Res. 266, 194–211. https://doi.org/10.1016/j.precamres.2015.05.021.
Martin, A.P., Condon, D.J., Prave, A.R., Lepland, A., 2013. A review of temporal constraints for the Palaeoproterozoic large, positive carbonate carbon isotope excursion (the Lomagundi–Jatuli Event). Earth Sci. Rev. 127, 242–261. https://doi.org/10.1016/j.earscirev.2013.10.006.
Massari, F., D'Alessandro, A., 2000. Tsunami-related scour-and-drape undulations in Middle Pliocene restricted-bay carbonate deposits (Salento, south Italy). Sedimentary Geology 135, 265–281. https://doi.org/10.1016/S0037-0738(00)00077-4.
Mastrogiacomo, G., Moretti, M., Owen, G., Spalluto, L., 2012. Tectonic triggering of slump sheets in the Upper Cretaceous carbonate succession of the Porto Selvaggio area (Salento peninsula, southern Italy): Synsedimentary tectonics in the Apulian Carbonate Platform. Sedimentary Geology 269–270, 15–27. https://doi.org/10.1016/j.sedgeo.2012.05.001.
Mayika, K.B., Moussavou, M., Prave, A.R., Lepland, A., Mbina, M., Kirsimäe, K., 2020. The Paleoproterozoic Francevillian succession of Gabon and the Lomagundi-Jatuli event. Geology 48, 1099–1104. https://doi.org/10.1130/G47651.1.
Mcllreath, I.A., James, N.P., 1978. Facies models 13. Carbonate slopes. Geoscience Canada 5 (4), 189–199.
Melezhik, V.A., Fallick, A.E., Medvedev, P.V., Makarikhin, V.V., 1999. Ga magnesite–stromatolite–dolomite–'red beds' association in a global context: a case for the world-wide signal enhanced by a local environment.
Merz-Preiß, M., Riding, R., 1999. Cyanobacterial tufa calcification in two freshwater streams: ambient environment, chemical thresholds and biological processes. Sed. Geol. 126, 103–124.
Mills, P.C., 1983. Genesis and diagnostic value of soft-sediment deformation structures—A review. Sedimentary Geology 35, 83–104. https://doi.org/10.1016/0037-0738(83)90046-5.
Myrow, P.M., Tice, L., Archuleta, B., Clark, B., Taylor, J.F., Ripperdan, R.L., 2004. Flat - pebble conglomerate: its multiple origins and relationship to metre - scale depositional cycles. Sedimentology 51, 973–996. https://doi.org/10.1111/j.1365-3091.2004.00657.x.
Nordeng, S.C., 1963. Precambrian Stromatolites as Indicators of Polar Shift1. In: Munyan, A.C. (Ed.), Polar Wandering and Continental Drift. SEPM Society for Sedimentary Geology, https://doi.org/10.2110/pec.63.01.0131.
Ojakangas, R.W., Morey, G.B., Southwick, D.L., 2001. Paleoproterozoic basin development and sedimentation in the Lake Superior region, North America. Sed. Geol. 141–142, 319–341. https://doi.org/10.1016/S0037-0738(01)00081-1.
Petryshyn, V.A., Corsetti, F.A., 2011. Analysis of growth directions of columnar stromatolites from Walker Lake, western Nevada: analysis of growth directions of columnar stromatolites. Geobiology 9, 425–435. https://doi.org/10.1111/j.1472-4669.2011.00293.x.
Pettijohn, F.J., 1943. Basal Huronian conglomerates of menominee and Calumet Districts, Michigan. J. Geol. 51, 387–397. https://doi.org/10.1086/625162.
Pettijohn, F.J., 1957. Paleocurrents of Lake Superior Precambrian quartzites. GSA Bull. 68, 469–480. https://doi.org/10.1130/0016-7606(1957)68[469:POLSPQ]2.0.CO;2.
Planavsky, N.J., Bekker, A., Hofmann, A., Owens, J.D., Lyons, T.W., 2012. Sulfur record of rising and falling marine oxygen and sulfate levels during the Lomagundi event. PNAS 109, 18300–18305. https://doi.org/10.1073/pnas.1120387109.
Pratt, B.R., 1984. Epiphyton and Renalcis; diagenetic microfossils from calcification of coccoid blue-green algae. J. Sediment. Res. 54, 948–971.
Prave, A.R., Kirsimäe, K., Lepland, A., Fallick, A.E., Kreitsmann, T., Deines, Y.E., Romashkin, A.E., Rychanchik, D.V., Medvedev, P.V., Moussavou, M., Bakakas, K., Hodgskiss, M.S.W., 2022. The grandest of them all: the Lomagundi–Jatuli Event and Earth's oxygenation. JGS 179, jgs2021-036. https://doi.org/10.1144/jgs2021-036.
Pruss, S.B., Bosak, T., Macdonald, F.A., McLane, M., Hoffman, P.F., 2010. Microbial facies in a Sturtian cap carbonate, the Rasthof Formation, Otavi Group, Northern Namibia. Precambr. Res. 181, 187–198.
Puffett, W.P., 1974. Geology of the Negaunee Quadrangle, Marquette County, Michigan. U.S. Geol. Surv. Prof. Paper 788. https://doi.org/10.3133/pp788.
Rasmussen, B., Zi, J., Bekker, A., 2024. New U-Pb zircon tuff ages and revised stratigraphic correlations in the Superior craton during the Great Oxidation Episode. Earth Planet. Sci. Lett. 640, 118779. https://doi.org/10.1016/j.epsl.2024.118779.
Richardson Jr., E.S., 1949. Some lower Huronian stromatolites of northern Michigan. Fieldiana Geol. 10 (8), 47–62.
Riding, R., 1991. Classification of microbial carbonates. In: Riding, Robert (Ed.), Calcareous Algae and Stromatolites. Springer, Berlin, Heidelberg, pp. 21–51. https://doi.org/10.1007/978-3-642-52335-9_2.

Riding, R., 2000. Microbial carbonates: the geological record of calcified bacterial-algal mats and biofilms: Microbial carbonates. Sedimentology 47, 179–214. https://doi.org/10.1046/j.1365-3091.2000.00003.x.
Rowland, S.M., Shapiro, R.S., 2002. Reef patterns and environmental influences in the Cambrian and earliest Ordovician.
Schidlowski, M., 1985. Carbon isotope discrepancy between Precambrian stromatolites and their modern analogs: inferences from hypersaline microbial mats of the Sinai coast. Orig. Life Evol. Biosph. 15, 263–277.
Schidlowski, M., Eichmann, R., Junge, C.E., 1975. Precambrian sedimentary carbonates: carbon and oxygen isotope geochemistry and implications for the terrestrial oxygen budget. Precambr. Res. 2, 1–69. https://doi.org/10.1016/0301-9268(75)90018-2.
Schidlowski, M., Eichmann, R., Junge, C.E., 1976. Carbon isotope geochemistry of the Precambrian Lomagundi carbonate province, Rhodesia. Geochim. Cosmochim. Acta 40, 449–455. https://doi.org/10.1016/0016-7037(76)90010-7.
Schlager, W., Chermak, A., 1979. Sediment Facies of Platform-Basin Transition, Tongue of the Ocean, Bahamas. In: Doyle, L.J., Pilkey, O.H. (Eds.), Geology of Continental Slopes. SEPM Society for Sedimentary Geology. https://doi.org/10.2110/pec.79.27.0193.
Schlager, W., Ginsburg, R.N., 1981. Bahama carbonate platforms — The deep and the past. Marine Geology, Carbonate Platforms of the Passive-type Continental Margins: Present and Past 44, 1–24. https://doi.org/10.1016/0025-3227(81)90111-0.
Schneider, D.A., Bickford, M.E., Cannon, W.F., Schulz, K.J., Hamilton, M.A., 2002. Age of volcanic rocks and syndepositional iron formations, Marquette Range Supergroup: implications for the tectonic setting of Paleoproterozoic iron formations of the Lake Superior region. Can. J. Earth Sci. 39, 999–1012. https://doi.org/10.1139/e02-016.
Sepkoski Jr., J.J., 1982. Flat-pebble conglomerates, storm deposits, and the cambrian bottom fauna. In: Einsele, G., Seilacher, A. (Eds.), Cyclic and Event Stratification. Springer Berlin Heidelberg, Berlin, Heidelberg, pp. 371–385. https://doi.org/10.1007/978-3-642-75829-4_28.
Sepkoski Jr, J.J., Bambach, R., Droser, M.L., 1991. Secular Changes in Phanerozoic Event Bedding and the Biological Overprint. In: Einsele, G., Ricken, W., Seilacher, A. (Eds.), Cyclic and Event Stratification, 2nd edition. Springer Verlag, Berlin, pp. 298–312.
Shapiro, R.S., Rigby, J.K., 2004. First occurrence of an in situ anthaspidellid sponge in a dendrolite mound (Upper Cambrian; Great Basin, USA). J. Paleo. 78, 645–650.
Shields, G., Veizer, J., 2002. Precambrian marine carbonate isotope database: Version 1.1. Geochemistry, geophysics, Geosystems 3, 1 of 12–12 12. https://doi.org/10.1029/2001GC000266.
Simone, L., 1980. Ooids: a review. Earth Sci. Rev. 16, 319–355.
Smith, B.P., Ingalls, M., Trower, E.J., Lingappa, U.F., Present, T.M., Magyar, J.S., Fischer, W.W., 2020. Physical controls on carbonate intraclasts: modern flat pebbles from Great Salt Lake, Utah. JGR Earth Surf. 125, e2020JF005733. https://doi.org/10.1029/2020JF005733.
Spalluto, L., Moretti, M., Festa, V., Tropeano, M., 2007. Seismically-induced slumps in Lower-Maastrichtian peritidal carbonates of the Apulian Platform (southern Italy). Sedimentary Geology, Deformation of soft sediments in nature and laboratory 196, 81–98. https://doi.org/10.1016/j.sedgeo.2006.06.009.
Stal, L.J., 2012. Cyanobacterial mats and stromatolites. In: Ecology of Cyanobacteria II: Their Diversity in Space and Time. Springer, pp. 65–125.
Stiller, M., Rounick, J.S., Shasha, S., 1985. Extreme carbon-isotope enrichments in evaporating brines. Nature 316, 434–435. https://doi.org/10.1038/316434a0.
Sumner, D.Y., 2024. Oxygenation of Earth's atmosphere induced metabolic and ecologic transformations recorded in the Lomagundi-Jatuli carbon isotopic excursion. Appl Environ Microbiol 90, e00093-24. https://doi.org/10.1128/aem.00093-24.
Suosaari, E.P., Awramik, S.M., Reid, R.P., Stolz, J.F., Grey, K., 2018. Living dendrolitic microbial mats in hamelin pool, Shark Bay, Western Australia. Geosciences 8, 212.
Swart, P.K., 2008. Global synchronous changes in the carbon isotopic composition of carbonate sediments unrelated to changes in the global carbon cycle. Proceedings of the National Academy of Sciences 105, 13741–13745. https://doi.org/10.1073/pnas.0802841105.
Swart, P.K., Reijmer, J.J., Otto, R., 2009. A re-evaluation of facies on great Bahama bank II: Variations in the δ13C, δ18O and mineralogy of surface sediments. Perspectives in carbonate geology: A tribute to the career of Robert Nathan Ginsburg, pp. 47–59.
Switzer, A.D., Jones, B.G., 2008. Large-scale washover sedimentation in a freshwater lagoon from the southeast Australian coast: sea-level change, tsunami or exceptionally large storm? The Holocene 18, 787–803. https://doi.org/10.1177/0959683608089214.
Tang, M., Chu, X., Hao, J., Shen, B., 2021. Orogenic quiescence in Earth's middle age. Science 371, 728–731. https://doi.org/10.1126/science.abf1876.
Tarhan, L.G., 2018. The early Paleozoic development of bioturbation—evolutionary and geobiological consequences. Earth Sci. Rev. 178, 177–207. https://doi.org/10.1016/j.earscirev.2018.01.011.
Taylor, G.L., 1972. Stratigraphy, sedimentology, and sulfide mineralization of the Kona Dolomite. (Ph.D. Thesis). Michigan Technical Institute, Houghton.
Tosti, F., Riding, R., 2017a. Current molded, storm damaged, sinuous columnar stromatolites: mesoproterozoic of northern China. Palaeogeogr. Palaeoclimatol. Palaeoecol. 465, 93–102. https://doi.org/10.1016/j.palaeo.2016.10.019.
Tosti, F., Riding, R., 2017b. Fine-grained agglutinated elongate columnar stromatolites: Tieling Formation, ca 1420 Ma, North China. Sedimentology 64, 871–902. https://doi.org/10.1111/sed.12336.
Trow, J.W., 1948. The Sturgeon Qurtzite of the Menominee District, Michigan. Ph.D. Thesis. University of Chicago, Chicago.
Twenhofel, W.H., 1919. Pre-Cambrian and carboniferous algal deposits. Am. J. Sci. 4, 339–352. https://doi.org/10.2475/ajs.s4-48.287.339.
Vallini, D.A., Cannon, W.F., Schulz, K.J., 2006. Age constraints for Paleoproterozoic glaciation in the Lake Superior Region: detrital zircon and hydrothermal xenotime ages for the Chocolay Group, Marquette Range Supergroup. Can. J. Earth Sci. 43, 571–591. https://doi.org/10.1139/e06-010.
van Loon, A.J., 2009. Soft-sediment deformation structures in siliciclastic sediments: an overview. Geologos 15, 3–55.
Veizer, J., 1983. Trace elements and isotopesin sedimentary carbonates. In: Reeder, R.J. (Ed.), Carbonates. De Gruyter, pp. 265–300. https://doi.org/10.1515/9781501508134-012.
Wohlabaugh, N., Mancuso, J., 1990. Depositional and diagenetic history of the big Cusp Algal Dolomite, Kona Formation, Marquette Range, Michigan. The Compass 67, 84–93.
Young, G.M., 1983. Tectono-sedimentary history of early Proterozoic rocks of the northern Great Lakes region. In: Medaris, L.G., Jr. (Ed.), Early Proterozoic Geology of the Great Lakes Region. Geological Society of America. https://doi.org/10.1130/MEM160-p15.